

# DISPERSAL AND GROWTH OF BACTERIA

Cover image by S. Gude.

PhD Thesis, Technische Universiteit Delft, 11.04.2016

*Dispersal and Growth of Bacteria*

Sebastian GUDE

ISBN 978-94-92323-03-3

A digital version of this thesis can be downloaded from <http://www.amolf.nl>.

# DISPERSAL AND GROWTH OF BACTERIA

PROEFSCHRIFT

ter verkrijging van de graad van doctor  
aan de Technische Universiteit Delft,  
op gezag van de Rector Magnificus prof. ir. K.C.A.M. Luyben;  
voorzitter van het College voor Promoties,  
in het openbaar te verdedigen op  
maandag, 11.04.2016 om 12:30 uur

door

**Sebastian GUDE**

Master of Science  
Ludwig-Maximilians-Universität München, Duitsland  
geboren te Kassel, Duitsland

This dissertation has been approved by the

promotor: Prof. dr. ir S.J. Tans

Technische Universiteit Delft

FOM Institute AMOLF

promotor: Prof. T.S. Shimizu, Ph.D.

Vrije Universiteit Amsterdam

FOM Institute AMOLF

Composition of the doctoral committee:

Rector Magnificus

chairman

Independent members:

Prof. dr. C. Dekker

Technische Universiteit Delft

Prof. P. B. Rainey, Ph.D.

New Zealand Institute for Advanced Study

Prof. E. T. Kiers, Ph.D.

Vrije Universiteit Amsterdam

H. O. Youk, Ph.D.

Technische Universiteit Delft

Dr. D. E. Rozen

Universiteit Leiden

Prof. dr. ir. M. C. M. van Loosdrecht

Technische Universiteit Delft, reserve member

The work described in this thesis is part of the research program of the  
Stichting voor Fundamenteel Onderzoek der Materie (FOM)  
which is financially supported by the  
Nederlandse Organisatie voor Wetenschappelijke Onderzoek (NWO).

This work was carried out at the

*FOM Institute AMOLF*

*Amsterdam*

where a limited number of copies of this dissertation is available.

---

# Contents

<b>1</b>	<b>Introduction</b>	<b>7</b>
	References	9
<b>2</b>	<b>Evolutionary constraints in variable environments, from proteins to networks</b>	<b>11</b>
2.1	Epistasis in variable environments	11
2.2	Epistasis within a regulatory protein	14
2.3	Natural evolution in changing environments	17
2.4	Constraints in cellular networks	19
2.5	Concluding remarks	21
	References	23
<b>3</b>	<b>Microbial diversity promoted by spontaneous spatial segregation</b>	<b>27</b>
3.1	Dispersal can drastically alter competition outcome	27
3.2	Spatial confinement can explain altered competition outcome	31
3.3	Growth-dispersal trade-offs promote stable coexistence	33
3.4	Discussion	36
3.5	Methods	38
	References	53
<b>4</b>	<b>Growth in spatial habitats</b>	<b>57</b>
4.1	Effects of initial population size	57
4.2	Effects of initial population ratio	58
4.3	Effects of initial spatial profile	60
4.4	Discussion	61
4.5	Methods	62
	References	63

<b>5</b>	<b>Microfabricated polyacrylamide devices for the controlled culture of growing cells and developing organisms</b>	<b>65</b>
5.1	Introduction	65
5.2	Microfabrication of polyacrylamide gels	67
5.3	Experimental designs	68
5.4	Temporal and spatial control of the microenvironment	70
5.5	Carbon controlled growth of bacteria	70
5.6	Temporary depolymerization of microtubules in yeast by a drug	73
5.7	Growth and development of spatially confined <i>C. elegans</i> larvae	74
5.8	Discussion	75
5.9	Methods	77
	References	83
	<b>Conclusion</b>	<b>87</b>
	<b>Summary</b>	<b>89</b>
	References	91
	<b>Samenvatting</b>	<b>93</b>
	<b>About the author</b>	<b>95</b>

# 1

---

## Introduction

Natural selection is the key driver of Darwinian evolution[1]. Darwin inferred the cause of evolution by comparing wild life observations made during his voyage on board the HMS Beagle with the outcome of animal breeding in his native England. Phenotypic variation, differential fitness, heritability of fitness and the fact that more offsprings are produced than can survive lead naturally to enrichment of phenotypes by chance better adapted to their current environment[2]. Fitness is increased by enhanced survival and exalted fecundity. However, measuring reproductive fitness in higher animals is hindered by their complex makeup and long life spans. Surveys of microbes, enabled by advances in molecular biology, overcome these obstacles[3] and open the way to rigorously probe the selective pressures shaping evolutionary dynamics.

This thesis starts with reviewing recent progress made in understanding constraints shaping evolutionary trajectories (chapter 2). Interactions among genes as well as interactions between genes and the environment can strongly influence the evolvability of traits. These epistatic effects are discussed on three different levels: single genes, single organisms and networks of genes. Subsequently the effect of space and dispersal on population dynamics is experimentally investigated in bacterial populations (chapter 3 and 4). Motile populations are found to spontaneously spatially segregate under a wide range of conditions, thus reshaping selective pressures drastically. Determinants of fitness, going beyond growth rate, are explored and successfully utilised to predict competition outcomes within a theoretical framework. Furthermore the altered selective pressures allow to elucidate stable coexistence[4–6] of motile organisms under a general set of prerequisites. The thesis ends with a description of a novel technique allowing to quantitatively probe microorganisms under well-defined conditions (chapter 5). By employing photolithography and molding to structure PDMS and polyacrylamide gels a wide

## 1 Introduction

---

range of microorganisms, from bacteria over yeast to nematodes, can be studied while their local environment is kept under precise control.



## References

- [1] C. R. Darwin, *On the Origin of Species by Means of Natural Selection, or the Preservation of Favoured Races in the Struggle for Life*, London: John Murray, 1859.
- [2] R. C. Lewontin, *The units of selection*, Annual review of ecology and systematics , 1 (1970).
- [3] S. F. Elena and R. E. Lenski, *Evolution experiments with microorganisms: the dynamics and genetic bases of adaptation*, Nature Reviews Genetics **4**, 457 (2003).
- [4] G. E. Hutchinson, *The paradox of the plankton*, American Naturalist , 137 (1961).
- [5] B. R. Levin, *Coexistence of two asexual strains on a single resource*, Science **175**, 1272 (1972).
- [6] R. A. Armstrong and R. McGehee, *Competitive exclusion*, American Naturalist , 151 (1980).

## REFERENCES

---

---

## Evolutionary constraints in variable environments, from proteins to networks

Environmental changes can not only trigger a regulatory response, but also impose evolutionary pressures that can modify the underlying regulatory network. Here, we review recent approaches that are beginning to disentangle this complex interplay between regulatory and evolutionary responses. Systematic genetic reconstructions have shown how evolutionary constraints arise from epistatic interactions between mutations in fixed environments. This approach is now being extended to more complex environments and systems. The first results suggest that epistasis is affected dramatically by environmental changes and, hence, can profoundly affect the course of evolution. Thus, external environments not only define the selection of favored phenotypes, but also affect the internal constraints that can limit the evolution of these phenotypes. These findings also raise new questions relating to the conditions for evolutionary transitions and the evolutionary potential of regulatory networks.

### 2.1 Epistasis in variable environments

Evolutionary adaptation is commonly thought of in terms of two distinct factors. On the one hand, external selective environments drive evolution to particular favored phenotypes, whereas, on the other hand, internal organismal constraints limit access to these phenotypes. Generally, evolution may be limited by physicochemical constraints[1] or by genetic exigencies[2], for instance when rare combinations of mutations are required for a functional change. In laboratory experiments,

---

The content of this chapter has been previously published as "Katja M. Taute, Sebastian Gude, Philippe Nghe, and Sander J. Tans - Evolutionary constraints in variable environments, from proteins to networks, Trends in Genetics, May 2014, Vol. 30, No. 5"

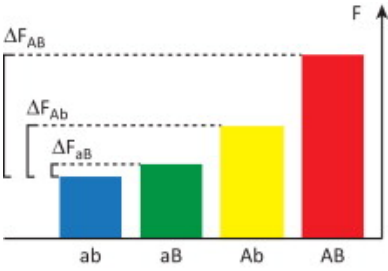
selection and constraint have been quantified for environments and phenotypes that are constant in time[3–7]. In comparison, little is known about selection and constraint in variable environments. The effects of environmental variability could be significant: different environments may not only favor different phenotypes, but also give rise to different evolutionary constraints and, hence, blur the line between the external and internal factors that determine evolutionary adaptation.

These issues are of general relevance given the variable character of natural environments. They are important for regulatory systems in particular. Regulatory systems may well experience selection and evolve in constant conditions, but their ability to respond to environmental changes is logically considered to be shaped by a history of selection in changing environments[8]. However, the mechanisms of regulatory evolution in variable environments remain incompletely understood, despite detailed insights into function[9–11] and sequence evolution[12–16]. Elucidating these questions will be central to understanding how the complex regulatory circuitries of cells have evolved, may offer routes to engineer synthetic regulatory functions, and provide new perspectives on the function of regulatory networks.

At the most elementary level, genetic constraints in constant environments can be expressed in terms of the interaction between two mutations, which is commonly referred to as epistasis (Table 2.1). For instance, a reconstruction of neighboring genotypes of the protein  $\beta$ -lactamase revealed that mutating a particular residue could increase resistance to antibiotics, but only if a second residue was mutated first, otherwise the resistance decreased[4, 17]. Such sign-epistatic interactions[5–7] can result from the highly integrated nature of molecular structures[18] and the interplay between protein stability and catalytic activity[19]. Sign epistasis affects selection, because fitness-increasing mutations are more readily fixed than neutral or fitness-decreasing mutations. In particular, the mutations will then be fixed in a specific order. Thus, sign-epistatic interactions between functionally important mutations constrain the number of mutational pathways accessible by positive selection. By contrast, forms of epistasis without changes in the sign of the effect, such as positive or negative epistasis (Table 2.1), do not have such drastic effects on selection, although they do provide important insights into functional relations.

The number of paths accessible by positive selection may also reduce to zero. Such a lack of available positively selected mutations could underlie cases of prolonged evolutionary stasis, and can be visualized as entrapment on a suboptimal fitness peak in genotype space[2]. Escape from such evolutionary stasis does remain possible in principle, for instance when multiple mutations are jointly fixed[4, 20], or when population expansion limits selection and maintains less fit phenotypes[6], although at much reduced probability. It has been shown on theoretical grounds that, for systems to display this more severe genetic constraint, they must exhibit reciprocal sign-epistatic interactions (Table 2.1)[21]. In this case, two mutations are jointly beneficial but each individually deleterious. Such interactions have been observed in the regulator MSN Three Homolog 1 (MTH1) and transporters hexose transporter 6 and 7 (HXT6 and HXT7) of the yeast glucose utilization pathway[22],

## 2.1 Epistasis in variable environments

Type of epistasis	Evolutionary consequences
No epistasis: $\Delta F_{AB} = \Delta F_{Ab} + \Delta F_{aB}$	Both paths from ab to AB are accessible by positive selection.
Magnitude epistasis: $\Delta F_{Ab}, \Delta F_{aB} > 0$	
Positive: $\Delta F_{AB} > \Delta F_{Ab} + \Delta F_{aB}$	Both paths from ab to AB are accessible by positive selection; if the effect is strong, multiple mutations are required to confer a large fitness increase.
Negative: $\Delta F_{AB} < \Delta F_{Ab} + \Delta F_{aB}$	Both paths from ab to AB are accessible by positive selection; the contribution of successive mutations to fitness becomes less and less (diminishing returns), which slows down adaptation.
Sign epistasis: $\Delta F_{Ab} < 0$ XOR $\Delta F_{aB} < 0$	One path is accessible by positive selection, whereas the other is not; hence, a particular order of mutations is favored.
Reciprocal sign epistasis: $\Delta F_{Ab} < 0$ AND $\Delta F_{aB} < 0$	Both paths from ab to AB are inaccessible by positive selection; this is a necessary condition for the existence of multiple local optima.
	Figure T1. Types of epistasis in constant environments and their evolutionary consequences. Between genotypes ab and the fitness optimum AB, two mutational paths are possible: via Ab and via aB. $\Delta F_{Ab}$ , $\Delta F_{aB}$ , and $\Delta F_{AB}$ are the fitness changes relative to the fitness of ab. We note that, because neutral mutations are not positively selected, conditionally neutral mutations ( $\Delta F_{Ab} = 0$ OR $\Delta F_{aB} = 0$ ) can be considered to exhibit (reciprocal) sign epistasis rather than magnitude epistasis.

**Table 2.1: Types of epistasis**

among other systems[23].

An emerging question is how epistasis and constraint are affected by environmental variability. Not only is the natural environment intrinsically variable, but the effects of mutations are also often found to depend strongly on the environment. For instance, the change in growth rate for different *Escherichia coli* Tn10 transposon mutants was found to depend on not only the genetic background, but also the type of growth media used[24]. Such interactions between genetic and environmental changes are pervasive in biological systems[25–30]. These observations raise the

question of how epistasis itself is impacted by environmental variability. Here, we review recent efforts that aim to address these issues. The approaches are diverse and range from the detailed analysis of interactions between genetic changes and environmental changes in a model transcription factor, to whole-genome investigations of epistatic interactions in complex networks, and exploit ideas from synthetic biology, experimental evolution, and mathematical modeling of cellular networks. These first studies revealed that environmental changes can drastically alter the interaction between two mutations, such that evolutionary paths can switch between being accessible to being inaccessible. At the scale of networks, certain epistatic effects are beginning to be understood mechanistically. The results pave the way to elucidating the evolution of regulatory networks based on a functional understanding of genetic and environmental interactions.

## 2.2 Epistasis within a regulatory protein

Transcriptional regulation is one of the simplest regulatory mechanisms within cells and, therefore, is a good starting point to explore the interplay between genetic and environmental changes. A recent study[31] zoomed in on one of the best-understood model systems for transcriptional regulation, the *E. coli* lac-repressor (Figure 2.2A). The authors had previously used experimental evolution to produce inverse LacI variants[32]. In contrast to the wild type repressor LacI<sub>WT</sub>, these LacI<sub>Inv</sub> mutants repressed the lac genes in the presence of the ligand isopropyl- $\beta$ -D-thiogalactopyranoside (IPTG), rather than in its absence. The genetic basis of the inverse response could be traced to three amino acid substitutions within the protein. Fixating these mutations involved a variable selection that alternated between favoring expression and repression of the downstream genes.

This scenario contains the basic ingredients for the adaptive evolution of regulatory responses: a succession of genetic and environmental changes in time. An elementary question that then arises is how these changes relate to each other. If these two types of change do not interact (meaning that their effects on phenotype or fitness are independent), then the specific pattern of environmental changes is immaterial to the genetic obstacles to evolution. However, if they do interact, obstacles that exist in one environment could be lifted in another (Figure 2.1). Hence, insight into the environment  $\times$  genotype interdependencies as well as the precise patterns of environmental change may be critical to understand the evolutionary adaptation of regulatory systems. Note that, in general, organisms may well fail to show adaptive evolution of regulatory responses to multiple environments and, for instance, rather evolve the same phenotypic change across all environments. To explore these issues, all single and double mutants were constructed for three inverse LacI variants that had been isolated, and their lac operon expression was assayed with and without IPTG.

The analysis showed a drastic effect of the environment on the genetic interactions

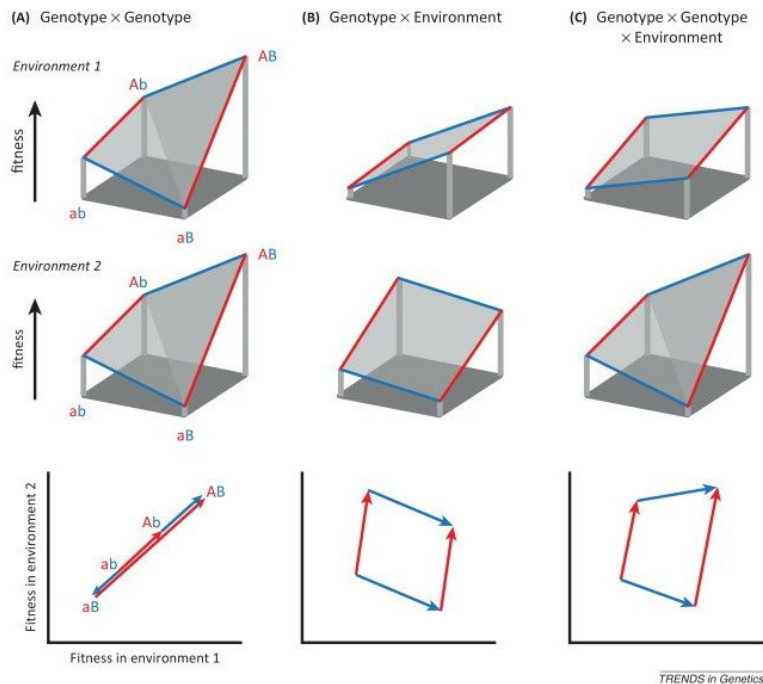


**Figure 2.1: Interdependencies between genotypes (G) and environment (E).**

The first two rows indicate phenotype or fitness for the elementary genotypes  $aa$ ,  $aB$ ,  $Ab$ , and  $AB$  in two environments, where capital denotes a genetic change. The bottom row indicates the same situations, but expressed as vectors in the two-environment fitness space. (A) GxG interactions: the effect of a mutation ( $b$  to  $B$ ) changes sign when switching to a different genetic backgrounds, but remains invariant under environmental changes. Mutation  $B$  is detrimental when applied to  $ab$ , but beneficial when applied to  $Ab$ . (B) GxE interactions: the effect of mutations is identical for different genetic backgrounds, but depends on the environment. In the upper two panels, slopes of opposing lines are identical but are altered by the environment, resulting in a parallelogram in the bottom vector plot. (C) GxGxE interactions: the effect of a mutation depends on the genetic background as well as the environment. As a result, the type of epistasis is different in both environments. This example shows a change from magnitude epistasis in environment 1 to sign epistasis in environment 2.

between pairs of mutations. For half of the pairs, an environmental change turned magnitude epistasis into sign epistasis. Take, for instance, the mutations T258A, which is positioned at the dimerization interface, and S97P, which is positioned in a region where bonds are formed and broken during the LacI conformational change that occurs upon ligand binding. When added to a third mutation, these genetic changes produced an inversion effect (Figure 2.2). Without IPTG, T258A and S97P were individually neutral, but jointly produced the required large expression increase. With IPTG, the situation was almost the opposite, because T258A individually increased expression, but was neutral when occurring after S97P. S97P here only decreased expression regardless of T258A. The particular positions of these

mutations do not readily provide clues to understand this interaction, or how they produce inversion. More generally, the complexity of such higher-order interactions between the environment and genotypes is difficult to grasp intuitively.

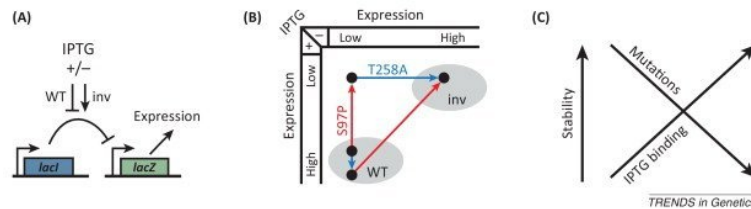


**Figure 2.2: Epistasis and environmental change in the LacI transcriptional regulator.** (A) Schematic illustration of the synthetic operon and its regulation system. Isopropyl- $\beta$ -D-thiogalactopyranoside (IPTG) is an inducer for the wild type (WT) LacI repressor and a co-repressor for the evolved inverse (inv) LacI repressor. (B) LacI mutations displaying genotype X genotype X environment (GxGxE) interactions (Figure 2.1, panel C). Prior to S97P, T258A increases LacZ expression, but only in the presence of IPTG. After S97P, the same mutation again increases expression, but now only in the absence of IPTG. (C) Proposed mechanistic explanation of the inversion and the higher-order GxGxE interactions. First, S97P disrupts the allosteric transition and locks LacI in the DNA-bound state. All mutations decrease LacI stability, leading to increased LacZ expression without IPTG. Stability can be restored by IPTG binding, resulting in repression of LacZ expression.

However, the relative simplicity of the system did open the door to a mechanistic explanation of the observed inversion and the involved higher-order interactions (Figure 2.2C). First, the mutations were found to decrease overall structural stability, which may have little effect on function until a critical destabilization is reached[33–35]. Thus, both mutations individually had almost no effect on DNA binding or LacZ expression in the absence of IPTG, but jointly conferred enough destabilization to break down DNA binding and increase expression. Second, S97P is known to block the allosteric change and keep LacI in the DNA-binding conformation[36–38]. This explains why S97P is neutral without IPTG but confers an expression decrease with IPTG. Finally, the binding of IPTG can restore stability in the destabilized LacI and, hence, result in DNA binding and repression[31]. This analysis indicates that a combination of simple molecular effects can give rise to a complex pattern of interactions between mutations and environmental change.

The higher-order interactions can directly impact selection. For instance, the mutations T258A and S97P are beneficial only when occurring simultaneously in the absence of IPTG, which dramatically lowers their chance of fixation. By contrast, positive selection is opened up when switching to IPTG, because S97P is then individually beneficial. However, T258A is not beneficial with IPTG, and so another environmental switch is required to access inversion by positive selection. A note of caution is that selection acts on fitness and not on expression. At the same time, a monotonic relation between expression and fitness would not affect this qualitative



analysis. Thus, overall, the environment not only defines selective pressures, but can also modulate underlying genetic constraints.

Variable environments and epistasis can also have nonintuitive effects on the evolutionary dynamics in the absence of regulation. One example is the reversibility of evolution, which has been studied using the antibiotic resistance protein TEM  $\beta$ -lactamase[28]. Two environments containing different antibiotics, taxime or piperacillin with clavulanic acid, favored two different genotypes of TEM  $\beta$ -lactamase. Some evolutionary intermediates displayed trade-offs, meaning that they were only well adapted to one of the two environments. The data showed that such trade-offs can enable reverse evolution, because deleterious mutations in one environment became beneficial in the second environment. Nevertheless, it was observed that reversibility of evolution was limited. Even though all transitions containing only one mutation were found to be reversible, the same did not hold true in general: reversibility as well as the accessibility of evolutionary transitions decreased when the length of the mutational path increased.

### 2.3 Natural evolution in changing environments

Even though coping with changing environments is considered a central cellular function, laboratory experiments of evolution by competition have only just begun to address environmental variability. Long-term experimental evolution studies, such as those of Lenski and coworkers[39], are based on many replicates of serial transfers of a culture into fresh medium and have yielded a wealth of data[3]. More recently, the same group performed such serial transfer experiments while alternating between different carbon sources[40]. Replicate populations showed larger variations in fitness than those evolved in constant environments, indicating divergent evolution. This finding suggests that evolution in variable environments is more complex than in constant environments, and may allow for a larger variety of evolutionary trajectories to be sampled. Another serial transfer study in variable environments[41] revealed that, whereas the evolving lac regulatory system adapted quickly to constant environments, alternating environments produced only either overall expression changes or constitutive expression. This result suggests another added complication, namely that variable environments and the associated increased number of evolutionary objectives lead to more severe constraints.

An alternative solution to the challenge of survival in variable environments is the evolution of stochastic rather than regulated phenotype changes. Examples include bacterial persistence[42] and phase variation[43]. A serial transfer experiment[44] provided some insight into the evolution of phenotype switching. *Pseudomonas fluorescens* bacteria were subjected to a variable selection regime continually favoring the emergence of new phenotypes by excluding the phenotype dominating the previous selection round. Although one may expect such a selection regime to give rise to continuous innovation, two of the 12 replicates of the experiment instead

yielded "bet-hedging" genotypes that displayed stochastic switching between two distinct phenotypes. This finding is reminiscent of the phenotype switching driven by highly mutable loci that is observed in various pathogens, often speculated to be a bet-hedging response to evade the immune system[43].

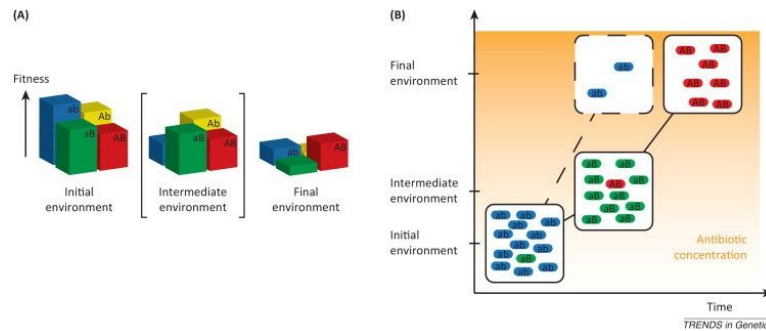


**Figure 2.3: Historical contingency upon an intermediate environment.** (A) Consider mutational trajectories from the ancestor genotype *ab* to *AB* via the intermediates *aB* or *Ab*. *ab* is fitter than its neighbors in the initial and final environment, but *AB* is fitter than either in the final environment. If no intermediate environment is provided in which *aB* or *Ab* will be positively selected over the initial genotype *ab*, then these two trajectories to *AB* are not selectively accessible. They are historically contingent upon the intermediate environment. (B) The demographics of an example population moved from the initial to the final environment either with (solid lines) or without time spent in the intermediate environment (broken lines). In the latter case (broken lines), the most successful genotype for the final environment cannot evolve.

Fluctuating selection is relevant in ecosystems subject to variations such as diurnal, tidal, or seasonal cycles, intermittent nutrient availability, or rare catastrophic events. Ecosystems may also be subject to gradual change, for instance as a result of resource depletion, pollution, or climate change. The rate of environmental change has been shown to affect survival of *E. coli* populations in an experimental evolution assay[29]. Replicate populations underwent serial dilutions into media with a gradually increasing concentration of an antibiotic. Under such conditions where mutations are rare and selection is strong, every single mutation must be beneficial to be retained. Thus, mutational trajectories are selectively accessible only if they comprise a series of single mutations, each of which increases fitness. Similar to previous work[45–48], fewer population extinctions were found for lower rates of environmental change. This finding is not surprising because demographics alone ensure that populations that spend more time under a lower concentration of antibiotic have more opportunity to produce beneficial mutations. However, by genetically tracing out the mutational trajectories of some of the successful lineages and measuring fitness for all intermediates in all environments, the authors showed that their experiment was dominated by a different mechanism: some of the mutational trajectories taken by the populations that successfully evolved through the slowly changing environment were "historically contingent" upon intermediate

environments. In essence, this means that the path taken is not selectively accessible without this intermediate environment (Figure 2.3). It was also shown that such historical contingencies not only require the gene X gene (GxG) effect of sign epistasis, but also a dependence of the sign of the fitness effect of a mutation on the environment (i.e., GxGxE).

In this study, the identification of relevant mutations was possible because the resistance-conferring mutations were limited to a single gene. The advent of next generation-sequencing methods will help to identify functionally relevant mutations that are distributed among different genes that function jointly within regulatory networks and, thus, enable similar approaches in more complex systems.

## 2.4 Constraints in cellular networks

We have so far mostly discussed genetic and environmental interactions at the level of individual genes. However, most cellular responses to environmental signals (from metabolism to chemotaxis to differentiation) rely on elaborate networks, which raises the issue of interdependencies between different genes. At the most elementary level, for instance, regulatory molecules that physically contact each other by a lock-and-key mechanism have been shown to give rise to intergenic epistasis[21, 49]. At a more systems level, epistatic interactions have been studied in metabolic networks, for instance. Here, we review these and other efforts to understand epistasis and evolutionary constraints in cellular networks, both from the modeling and experimental evolution perspectives.

One of the modeling approaches simulated the effects of single and double knockouts in yeast metabolism, using a flux balance analysis model[50]. Such models maximize the total flux among all possible solutions under known constraints of the system, the network topology being accounted for by stoichiometric relations. Here, interactions were classified into three categories: negative epistasis, no epistasis, or positive epistasis, corresponding to the deleterious effect of combined mutations being stronger, equal to, or weaker than the additive expectation, respectively. It was observed that the most relevant scale to classify epistasis was at the level of metabolic modules, defined as sets of genes that contribute to the same metabolic pathway, such as glycolysis or ATP synthesis. Even though interactions within modules contributed significantly to epistasis, most epistatic interactions were measured to occur between modules, suggesting the importance of functional relations between them. Moreover, these interactions were observed mainly between genes without known physical interactions. The central finding of this study was that, with few exceptions, genes from the same metabolic module had the same type of epistatic interaction with genes from another module. Conversely, the authors clustered genes by maximizing epistasis similarity between clusters and again found consistent functional sets, showing the independence of this finding from previous gene annotations.

Some of these key predictions were later verified by experimental screens of double mutants in yeast[51, 52]. The authors developed a protocol to infer fitness from colony size and measured the effect of several million double knockouts, including metabolic genes. They found that proteins participating in the same complex had mostly the same type of epistatic interactions with proteins from another complex. It was also confirmed that a large amount of epistasis occurred between genes that were not known to engage in direct physical interactions.

Evolution experiments have also produced evidence for the importance of functional interactions between genes in evolutionary trajectories. In one such study, the authors performed more than 100 parallel repeats of the adaptation of bacteria to elevated temperature[53], and they sequenced genomes of individuals randomly picked from each independent line of evolution. They found that only 2-3% of point mutations were shared between two or more lines, whereas the evolutionary patterns were reproducible at higher levels of organization in the cell. Indeed, mutations were strongly biased toward 12 functional modules, such as the RNA polymerase complex, the wall formation complex, the stress regulation genes, as well as specific metabolic pathways.

The dominance of these few functional modules in shaping the evolutionary trajectories was confirmed when looking at mutation distributions in more details. In fact, a majority of these modules contained a single mutation per line, which was significantly less than the random expectation. Moreover, when considering a given module across different lines, the observed single mutations affecting it were diverse, emphasizing the importance of functional modules as evolutionary units, rather than specific mutations within them. The authors interpreted the occurrence of a single mutation per module as negative epistasis, when the combined beneficial effect of two mutations was almost equal to the effect of only one mutation. In the simplest case, for instance, adaptation by inactivating a gene can be achieved by several mutations, but once one such damaging mutation is fixed, additional mutations in the same gene would be neutral and, hence, not be fixed. Note that such negative epistasis also appeared in situations where genes retained their function, pointing to additional mechanisms that remain to be explained. In any case, further adaptation could occur only by changes in other functional modules.

Two genes deviated from the general result and typically sustained more than two mutations per independent line. These were the transcription termination factor *rho* and the *rpoBC* operon, encoding subunits of the RNA polymerase. As suggested by the authors, the broad range of functions that these two genes affect explains the existence of several compensatory mutations. More importantly, mutations in these two genes were systematically accompanied by mutations in other modules, the set of modules associated with either *rho* or *rpoBC* having strikingly small overlap. This suggested the existence of a structured fitness landscape, with mutations occurring primarily in either *rho* or *rpoBC* constraining further evolution to separated evolutionary paths. The authors measured that these two paths led to the same level of fitness, further suggesting the existence of two local optima and sign or reciprocal

sign epistasis between these two exclusive sets of mutations. These findings are not isolated and other evolutionary studies have recently shown negative epistasis[54, 55] and sign or reciprocal sign epistasis[22, 56, 57] between genes within metabolic pathways or at a global level of organization in the cell.

Note that the existence of a relation between network structure and epistasis is not a priori obvious, because even simple network topologies can give rise to a variety of epistasis patterns depending on details of the network components[49, 58]. Such relations may in particular be averaged out when one tries to find correlations between epistasis and statistical quantifications of network complexity or local connectivity[58, 59], which may disregard some specific structures at intermediate and large scales of the network. By clustering genes, such specific structures were captured, eventually leading to the classification of epistasis patterns[50].

## 2.5 Concluding remarks

Environmental change and the genetic makeup of organisms are considered key to evolution. Indeed, biologists since Darwin have been intrigued by the emergence of novel regulatory functions in populations challenged by the conflicting demands of variable environments[60]. However, phenotypes that have been studied historically have been too complex to link environment and genetics at the molecular level. Here, we have provided some insight into how these obstacles are now being overcome by new approaches that combine modern genetics and synthetic biology with an appreciation of simple model systems. The first results indicate not only that biological systems display pervasive interdependencies, but that these interdependencies can also critically affect their evolution. Changes in the environment do not merely affect the magnitude of genetic epistasis, but can completely reshuffle genetic interactions. As a result, evolutionary paths that are blocked in one environment can be opened up in another and, vice versa, paths that are accessible in one environment can become blocked in another. Thus, environmental change can drive evolutionary transitions by altering genetic interactions.

The pervasiveness of ExG interactions raises many questions. For instance, patterns of environmental variation are ecologically diverse, ranging from gradual changes to stochastic fluctuations and spatial structured variations. These patterns can produce diverse evolutionary responses, consisting of gain or loss of regulatory abilities, bet-hedging, and impact on divergence within populations. Many open issues remain at the scale of regulatory networks, for instance on the relation between functional and evolutionary constraints. So far, the focus has been on constant environments, leaving the regime of variable environments to be explored. Theoretical approaches are being developed that use a simplified phenotype-fitness mapping[61] or dynamic simulations of networks[62, 63] to assess epistasis. Such conceptual developments could be coupled with targeted network modifications and quantitative phenotypic assays[64]. Together, such efforts can provide a new

## 2 Evolutionary constraints in variable environments, from proteins to networks

perspective on the variety of observed regulatory functions and behavior, and allow for a quantitative understanding of evolution in complex environments.

## References

- [1] K. Dill et al., *Physical limits of cells and proteomes*, Proc. Natl. Acad. Sci. U.S.A. **108**, 17876 (2011).
- [2] S. Wright, *The roles of mutation, inbreeding, crossbreeding and selection in evolution*, Proc. Sixth Cong. Genet. **1**, 356 (1932).
- [3] S. Elena and R. Lenski, *Evolution experiments with microorganisms: the dynamics and genetic bases of adaptation*, Nat. Rev. Genet. **4**, 457 (2003).
- [4] D. Weinreich et al., *Darwinian evolution can follow only very few mutational paths to fitter proteins*, Science **312**, 111 (2006).
- [5] F. Poelwijk et al., *Empirical fitness landscapes reveal accessible evolutionary paths*, Nature **445**, 383 (2007).
- [6] D. Weinreich et al., *Perspective: sign epistasis and genetic constraint on evolutionary trajectories*, Evolution **59**, 1165 (2005).
- [7] J. Bridgham et al., *Evolution of hormone-receptor complexity by molecular exploitation*, Science **312**, 97 (2006).
- [8] M. Pigliucci, *Phenotypic Plasticity: Beyond Nature and Nurture*, John Hopkins University Press, 2001.
- [9] S. Gottesman, *Bacterial regulation: global regulatory networks*, Annu. Rev. Genet. **18**, 415 (1984).
- [10] D. Kern and E. Zuiderweg, *The role of dynamics in allosteric regulation*, Curr. Opin. Struct. Biol. **13**, 748 (2003).
- [11] S. Rosenfeld, *Mathematical descriptions of biochemical networks: stability, stochasticity, evolution*, Prog. Biophys. Mol. Biol. **106**, 400 (2011).
- [12] J. Riechmann et al., *Arabidopsis transcription factors: genome-wide comparative analysis among eukaryotes*, Science **290**, 2105 (2000).
- [13] W. Atchley and W. Fitch, *A natural classification of the basic helix-loop-helix class of transcription factors*, Proc. Natl. Acad. Sci. U.S.A. **94**, 5172 (1997).
- [14] M. Babu et al., *Structure and evolution of transcriptional regulatory networks*, Curr. Opin. Struct. Biol. **14**, 283 (2004).
- [15] R. Lusk and M. Eisen, *Evolutionary mirages: selection on binding site composition creates the illusion of conserved grammars in Drosophila enhancers*, PLoS Genet. **6**, e1000829 (2010).
- [16] P. Wittkopp and G. Kalay, *Cis-regulatory elements: molecular mechanisms and evolutionary processes underlying divergence*, Nat. Rev. Genet. **13**, 59 (2012).
- [17] F. Richards, *Areas, volumes, packing, and protein structure*, Annu. Rev. Biophys. Bioeng. **6**, 151 (1977).
- [18] D. Kirby et al., *Maintenance of pre-mRNA secondary structure by epistatic selection*, Proc. Natl. Acad. Sci. U.S.A. **92**, 9047 (1995).
- [19] M. DePristo et al., *Missense meanderings in sequence space: a biophysical view of protein evolution*, Nat. Rev. Genet. **6**, 678 (2005).
- [20] P. Phillips, *Waiting for a compensatory mutation: phase zero of the shifting-balance process*, Genet. Res. **67**, 271 (1996).
- [21] F. Poelwijk et al., *Reciprocal sign epistasis is a necessary condition for multi-peaked fitness landscapes*, J. Theor. Biol. **272**, 141 (2011).
- [22] D. Kvitck and G. Sherlock, *Reciprocal sign epistasis between frequently experimentally*

## REFERENCES

---

- evolved adaptive mutations causes a rugged fitness landscape*, PLoS Genet. **7**, e1002056 (2011).
- [23] J. de Visser et al., *Exploring the effect of sex on empirical fitness landscapes*, Am. Nat. **174** (Suppl. 1), S15 (2009).
- [24] S. Remold and R. Lenski, *Pervasive joint influence of epistasis and plasticity on mutational effects in Escherichia coli*, Nat. Genet. **36**, 423 (2004).
- [25] J. Kubinak et al., *Experimental viral evolution to specific host MHC genotypes reveals fitness and virulence trade-offs in alternative MHC types*, Proc. Natl. Acad. Sci. U.S.A. **109**, 3422 (2012).
- [26] T. Bataillon et al., *Cost of adaptation and fitness effects of beneficial mutations in Pseudomonas fluorescens*, Genetics **189**, 939 (2011).
- [27] S. Remold, *Understanding specialism when the Jack of all trades can be the master of all*, Proc. Biol. Sci. **279**, 4861 (2012).
- [28] L. Tan et al., *Hidden randomness between fitness landscapes limits reverse evolution*, Phys. Rev. Lett. **106**, 198102 (2011).
- [29] H. Lindsey et al., *Evolutionary rescue from extinction is contingent on a lower rate of environmental change*, Nature **494**, 463 (2013).
- [30] A. Hall et al., *The fitness cost of rifampicin resistance in Pseudomonas aeruginosa depends on demand for RNA polymerase*, Genetics **187**, 817 (2011).
- [31] M. de Vos et al., *Environmental dependence of genetic constraint*, PLoS Genet. **9**, e1003580 (2013).
- [32] F. Poelwijk et al., *Tradeoffs and optimality in the evolution of gene regulation*, Cell **146**, 462 (2011).
- [33] P. Chen and E. Shakhnovich, *Lethal mutagenesis in viruses and bacteria*, Genetics **183**, 639 (2009).
- [34] N. Tokuriki et al., *How protein stability and new functions trade off*, PLoS Comput. Biol. **4**, e1000002 (2008).
- [35] C. Wylie and E. Shakhnovich, *A biophysical protein folding model accounts for most mutational fitness effects in viruses*, Proc. Natl. Acad. Sci. U.S.A. **108**, 9916 (2011).
- [36] T. Flynn et al., *Allosteric transition pathways in the lactose repressor protein core domains: asymmetric motions in a homodimer*, Protein Sci. **12**, 2523 (2003).
- [37] H. Zhan et al., *Positions 94–98 of the lactose repressor Nsubdomain monomer–monomer interface are critical for allosteric communication*, Biochemistry **49**, 8636 (2010).
- [38] M. Lewis et al., *Crystal structure of the lactose operon repressor and its complexes with DNA and inducer*, Science **271**, 1247 (1996).
- [39] R. Lenski and M. Travisano, *Dynamics of adaptation and diversification: a 10,000-generation experiment with bacterial populations*, Proc. Natl. Acad. Sci. U.S.A. **91**, 6808 (1994).
- [40] T. Cooper and R. Lenski, *Experimental evolution with E. coli in diverse resource environments. I. Fluctuating environments promote divergence of replicate populations*, BMC Evol. Biol. **10**, 10 (2010).
- [41] F. Poelwijk et al., *Optimality and evolution of transcriptionally regulated gene expression*, BMC Syst. Biol. **5**, 128 (2011).
- [42] N. Balaban, *Persistence: mechanisms for triggering and enhancing phenotypic variability*, Curr. Opin. Genet. Dev. **21**, 768 (2011).



- [43] M. van der Woude and A. Baumler, *Phase and antigenic variation in bacteria*, Clin. Microbiol. Rev. **17**, 581 (2004).
- [44] H. Beaumont et al., *Experimental evolution of bet hedging*, Nature **462**, 90 (2009).
- [45] G. Perron et al., *The rate of environmental change drives adaptation to an antibiotic sink*, J. Evol. Biol. **21**, 1724 (2008).
- [46] G. Bell and A. Gonzalez, *Evolutionary rescue can prevent extinction following environmental change*, Ecol. Lett. **12**, 942 (2009).
- [47] S. Collins and J. de Meaux, *Adaptation to different rates of environmental change in Chlamydomonas*, Evolution **63**, 2952 (2009).
- [48] G. Bell and A. Gonzalez, *Adaptation and evolutionary rescue in metapopulations experiencing environmental deterioration*, Science **332**, 1327 (2011).
- [49] B. Lehner, *Molecular mechanisms of epistasis within and between genes*, Trends Genet. **27**, 323 (2011).
- [50] D. Segre et al., *Modular epistasis in yeast metabolism*, Nat. Genet. **37**, 77 (2005).
- [51] A. Baryshnikova et al., *Quantitative analysis of fitness and genetic interactions in yeast on a genome scale*, Nat. Methods **7**, 1017 (2010).
- [52] M. Costanzo et al., *The genetic landscape of a cell*, Science **327**, 425 (2010).
- [53] O. Tenaillon et al., *The molecular diversity of adaptive convergence*, Science **335**, 457 (2012).
- [54] A. Khan et al., *Negative epistasis between beneficial mutations in an evolving bacterial population*, Science **332**, 1193 (2011).
- [55] H.-H. Chou et al., *Diminishing returns epistasis among beneficial mutations decelerates adaptation*, Science **332**, 1190 (2011).
- [56] R. Woods et al., *Second-order selection for evolvability in a large Escherichia coli population*, Science **331**, 1433 (2011).
- [57] S. Damkiær et al., *Evolutionary remodeling of global regulatory networks during long-term bacterial adaptation to human hosts*, Proc. Natl. Acad. Sci. U.S.A. **110**, 7766 (2013).
- [58] A. Gjuvsland et al., *Statistical epistasis is a generic feature of gene regulatory networks*, Genetics **175**, 411 (2007).
- [59] J. Macía et al., *The causes of epistasis in genetic networks*, Evolution **66**, 586 (2012).
- [60] T. DeWitt and S. Scheiner, *Phenotypic Plasticity: Functional and Conceptual Approaches*, Oxford University Press, 2004.
- [61] H.-C. Chiu et al., *Epistasis from functional dependence of fitness on underlying traits*, Proc. Biol. Sci. **279**, 4156 (2012).
- [62] A. Pumir and B. Shraiman, *Epistasis in a model of molecular signal transduction*, PLoS Comput. Biol. **7**, e1001134 (2011).
- [63] J. Cotterell and J. Sharpe, *Mechanistic explanations for restricted evolutionary paths that emerge from gene regulatory networks*, PLoS ONE **8**, e61178 (2013).
- [64] G. Carter et al., *Prediction of phenotype and gene expression for combinations of mutations*, Mol. Syst. Biol. **3**, 96 (2007).

## REFERENCES

---

# 3

---

## Microbial diversity promoted by spontaneous spatial segregation

Explaining biodiversity is a central challenge in ecology[1–8]. It has long been thought that functional trade-offs can promote coexistence[9–12]. In particular, weak local resource competitors may be able to coexist with strong ones by more rapidly accessing distant resources[13–22], which often become available as discrete patches[23, 24]. Here we test these predictions empirically, by studying how mixed microbial populations colonise new resource patches. We find that fast-growing-slow-dispersing and slow-growing-fast-dispersing populations can reciprocally invade each other. Hence stable coexistence is attained. Mechanistically coexistence is explained by an efficient segregation into distinct spatial niches generated through an interplay of dispersal and competition for limiting nutrients. Since the mechanism does not rely on specific inter-species interactions such as chemical warfare[25–29] or cooperation[30, 31], it is in principle capable to act on very basic forms of life, e.g. those present during the early days of evolutionary history.

### **3.1 Dispersal can drastically alter competition outcome**

On a basic level many (micro-)organisms display growth[32–34] and motility[35, 36] (figure 3.1a). Here we investigate the impact of motility on competitions of microbial populations in spatial habitats. *Escherichia coli*, like many microbes, can perform taxis on environmental cues. Transmembrane receptor complexes in combination

---

The work presented in this chapter is a collaborative effort of Sebastian Gude, Katja M. Taute, Thomas S. Shimizu, and Sander J. Tans

### 3 Microbial diversity promoted by spontaneous spatial segregation

with an intracellular signalling network (Che proteins) and flagella enable directed dispersal[35] constituted by an interplay of active directed motility and growth. We start out by constructing a slower dispersing mutant from wild-type *Escherichia coli* by replacing its native response regulator gene *cheY* with the constantly active form *cheY* D13K Y106W (figure 3.1c and supplementary figure 3.4). The mutant population is no longer able to sense its local environment and hence disperses as a Fisher wave[37, 38] constituted by active random motility and growth.

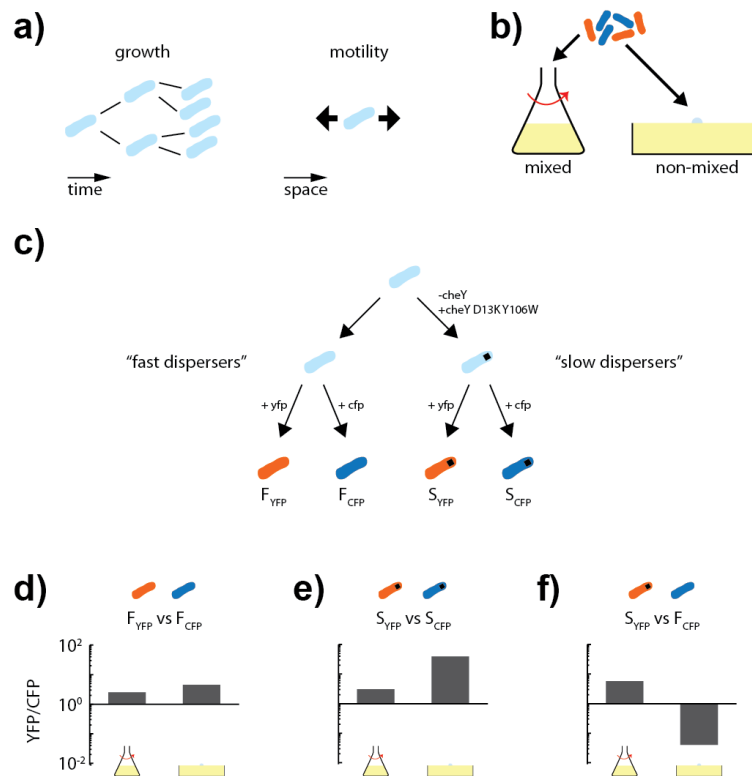


**Figure 3.1: Dispersal can drastically alter competition outcome.**

a) Illustration of growth and motility. b) Illustration of mixed (well-stirred) and non-mixed (spatially structured) environments. Dispersal, i.e. spreading of a bacterial colony in a spatially structured environment, is constituted by an interplay of growth and motility. c) Fast (F) and slow (S) dispersing populations. d-f) Competition outcomes obtained by fluorescence colony counting. Initial population ratio 1:1. Relative errors are of the order of 10-40%.

We evenly divide wild-type *Escherichia coli* into two subpopulations, F<sub>YFP</sub> and F<sub>CFP</sub>, labelled with YFP (yellow fluorescent protein) and CFP (cyan fluorescent protein), respectively. We investigate their competitive performance in a well-stirred (mixed) and in a spatially structured (non-mixed) environment, constituted by point-inoculating a population mixture[39] on soft agar plates, to explore potential differences in selective pressures enforced by environments with and without spatial context (figure 3.1b and d). After inoculation onto the surface of the soft agar plate

### 3.1 Dispersal can drastically alter competition outcome

---

bacteria migrate into the porous soft agar gel wherein they can grow and move. To obtain final population ratios we dissolve, dilute and transfer samples to hard agar plates and perform fluorescence-based colony counting (see Methods). As suggested by the slight growth rate advantage displayed by  $F_{YFP}$  (supplementary figure 3.4a),  $F_{YFP}$  increases about 2-fold over  $F_{CFP}$  in a mixed environment. As their dispersal rates are identical (supplementary figure 3.4b), the competition outcome on soft agar plates remains mainly unchanged compared to the mixed scenario. Next we compete the two slower dispersing populations,  $S_{YFP}$  and  $S_{CFP}$  (figure 3.1e). Again we find the population with the slightly higher growth rate,  $S_{YFP}$ , to increase in abundance in a mixed environment. The magnitude of the competition outcome on soft agar plates is drastically altered ( $\sim 10x$  larger compared to the mixed environment). Interestingly, when inoculated separately on soft agar plates  $S_{YFP}$  merely holds an area  $\sim 1.6x$  larger than that occupied by  $S_{CFP}$  after 4 days, the time frame of the corresponding competition experiment (see supplementary figure 3.5). Since the two populations are by construction identical in all respects except their respective fluorescent labels, and thus interspecies interaction[25–29] or nutrient specialisation[6] can be ruled out, we conclude that even seemingly small differences in dispersal rate such as displayed by  $S_{YFP}$  and  $S_{CFP}$  (supplementary figure 3.4b) can have a profound impact on the competition outcome of motile populations.

$S_{YFP}$  performs better than  $S_{CFP}$  in both growth and dispersal, but it remains unclear whether an advantage in dispersal can overcome a disadvantage in growth. Hence we compete two populations displaying a trade-off between growth and dispersal (figure 3.1f), namely  $S_{YFP}$  (slow disperser, fast grower) and  $F_{CFP}$  (fast disperser, slow grower). As previously the competition outcome in a mixed environment is in good agreement with the detected differences in growth rates (supplementary figure 3.4a).  $S_{YFP}$  outcompetes  $F_{CFP}$ . On soft agar plates, however, the competition outcome is inverted.  $F_{CFP}$ , the faster dispersing population, increases in abundance over  $S_{YFP}$ . A  $\sim 3$ -fold advantage in dispersal rate is found to overcompensate for a growth rate handicap of  $\sim 15\%$ , thus establishing dispersal rate as major determinant of competitive performance in spatial habitats.

### 3 Microbial diversity promoted by spontaneous spatial segregation

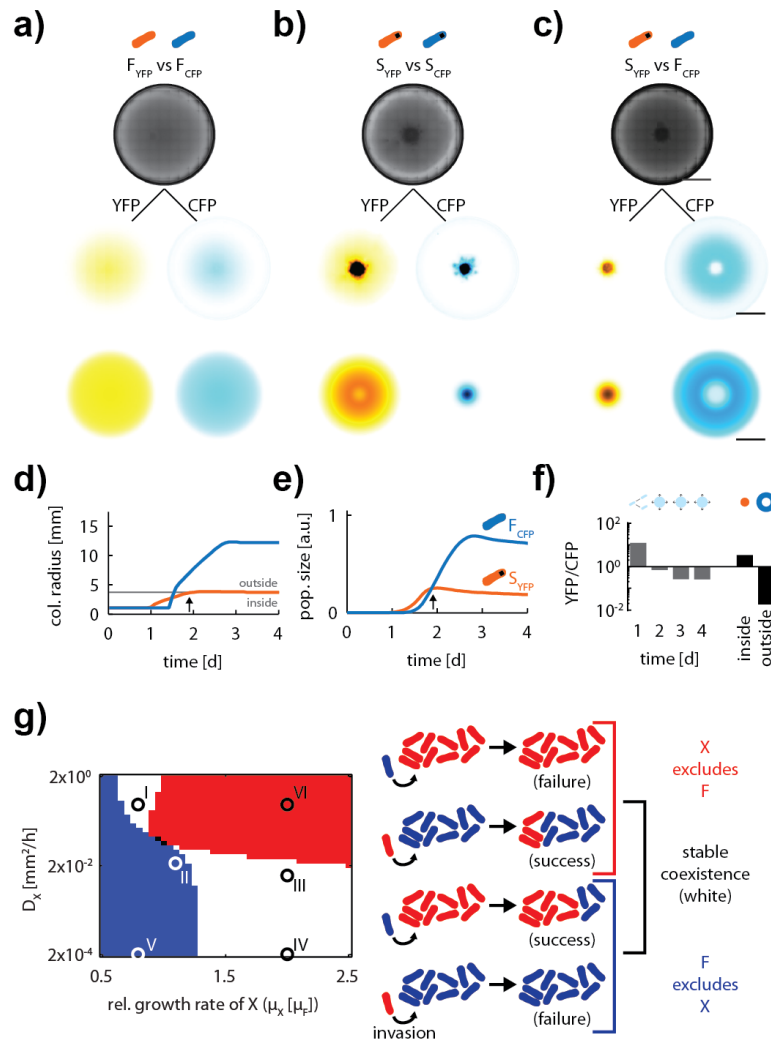


**Figure 3.2: Spatial confinement and niche segregation.**

a-c) Maps of bacterial distributions in brightfield (top), in fluorescence (middle) and as predicted by theory (bottom). Scale bars: 10 mm. In brightfield a dark ring marks the edges of the petri dish. Inside the petri dish darker regions correspond to higher bacterial densities. d-f) Temporal dynamics of  $S_{YFP}$  vs  $F_{CFP}$  extracted from fluorescence images.  $S_{YFP}$  (orange) and  $F_{CFP}$  (blue). d) Colony radius as function of time. e) Population size as function of time. f) Competition outcome as function of time and space. Inside / outside after 4 days as defined in panel d. g) Model predictions of stable community structures for F ( $= F_{YFP} \approx F_{CFP}$ ) vs X (dark blue: F excludes X, red: X excludes F, white: stable coexistence, black: unstable coexistence). Markers indicate parameter values used in supplementary figure 3.11.

## 3.2 Spatial confinement can explain altered competition outcome

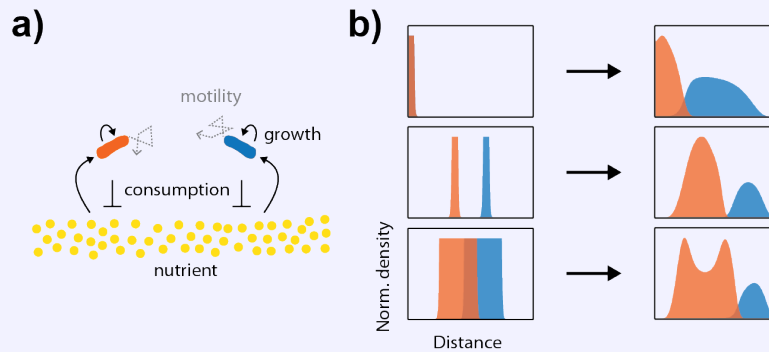
Aiming for a deeper understanding of the factors shaping competitive performance in spatial habitats, we record spatial population distributions after 4 days of competition on soft agar plates (figure 3.2a-c) in brightfield (top) and fluorescence (middle). Fluorescent labels allow us to decompose the overall spatial bacterial distribution into its two subpopulations, shown in yellow (YFP) and blue (CFP), respectively. While  $F_{YFP}$  and  $F_{CFP}$  have dispersed a similar distance in competition (figure 3.2a),  $S_{CFP}$  ( $S_{YFP}$  vs  $S_{CFP}$ ) and  $S_{YFP}$  ( $S_{YFP}$  vs  $F_{CFP}$ ) are found to be confined to a region considerably smaller than that of their faster dispersing competitors (figure 3.2b-c), with colony radii smaller than achieved when inoculated individually (compare with supplementary figure 3.5). We infer that faster-dispersing populations spatially confine slower-dispersing populations when inoculated in spatial environments (see also supplementary figures 3.6, 3.7 and 3.9). In addition, competitors displaying a growth-dispersal trade-off, as for  $S_{YFP}$  vs  $F_{CFP}$ , are found to spatially segregate into adjacent spatial regions, as seen in their dot-donut shaped colony morphologies (figure 3.2c). For the competitions without growth-dispersal trade-off ( $F_{YFP}$  vs  $F_{CFP}$  and  $S_{YFP}$  vs  $S_{CFP}$ ) both populations depict overlapping spatial distributions around the point of inoculation and hence do not exhibit spatial segregation. We are able to reproduce the observed spatial population distributions and competition outcomes on soft agar plates with a modified Keller-Segel model[40] (figure 3.2a-c, bottom), encompassing active dispersal and competition for a single diffusible nutrient (for further details see box 3.1 and Methods). Please note that spatial confinement is not caused by the tactic behaviour of the faster dispersing population, but is rather solely determined by differences in dispersal rate (see supplementary figure 3.9).

Intrigued by the observation of spontaneous spatial segregation, i.e. in the absence of predetermined environmental heterogeneities or external influences, we continue to investigate the competition dynamics of  $S_{YFP}$  vs  $F_{CFP}$  in more detail. Tracking population fronts of the two competitors over time (figure 3.2d) depicts both populations spreading out after an initial lag. While  $F_{CFP}$  continues to disperse until 60 hours after inoculation, dispersal of  $S_{YFP}$  stops after 48 hours.

Our model predicts the onset of nutrient depletion at the population front of  $S_{YFP}$  to coincide with the time point of its confinement (supplementary figure 3.8). To experimentally verify this prediction we employ calibrated fluorescence intensities to estimate population sizes over time (figure 3.2e, supplementary figure 3.13). We confirm that  $S_{YFP}$  becomes spatially confined around the same time as its overall growth ceases (black arrows in figure 3.2e-f). Hence we infer that the ability of  $F_{CFP}$  to access pristine territory at a faster rate enables it to act as a nutrient sink that surrounds  $S_{YFP}$ , causing the latter's dispersal and growth to stall. This effect has some similarities to nutrient depletion in the centre of large growing biofilm colonies[41].

#### Box 3.1: Competition model

We employ a modified version of a Keller-Segel model[40] in combination with a Monod growth term[32] and nutrient consumption to capture the competition dynamics (see Methods).



Schematic cartoon of the modelled interactions (panel a). The spatio-temporal nutrient distribution is modelled explicitly (diffusion coefficient  $D = 1.8 \text{ mm}^2/\text{h}$ ). Bacterial growth is coupled to the local nutrient concentration, and production of biomass coincides with nutrient consumption. Bacteria can move actively through their environment, by random movement or taxis along nutrient gradients. Active motility, like growth, is influenced by the local nutrient concentration, and ceases once the nutrient is locally depleted. The initial nutrient profile is set to be spatially homogeneous, while the initial bacterial distributions are concentrated into a point-like region, mimicking experimental conditions. There are no directed interactions between the bacterial populations. The competition model can reproduce the experimentally observed spatial patterns (figure 3.2a-c), with all parameter values fixed by independent experiments on single populations.

We use the competition model to explore a generic set of initial population distributions in one Cartesian dimension (panel b). Completely overlapping initial population distributions can segregate over time if the populations exhibit a growth-dispersal trade-off (top). Completely separated and partially overlapping initial population distributions can maintain their segregated nature (middle and bottom). In general spatial segregation allows individual populations to secure exclusive access to parts of the habitat and thus to the nutrients contained therein. As an example, when inoculated without overlap the orange and the blue population have prior access to the nutrients far left / right in the habitat, respectively. Hence the blue population can maintain its growth even after the orange population's growth stalled as a consequence of local nutrient depletion. For a discussion on different 2D geometries see supplementary figure 3.17.



Both experiment and the modelling reveal that the competition dynamics are composed of two distinct phases, an early one determined by growth and a later one determined by dispersal (figure 3.2f). During the growth dominated phase both populations compete locally for the same nutrient and hence  $S_{YFP}$  is seen to increase in abundance over  $F_{CFP}$  reflecting its growth rate advantage (day 1). For later times the faster dispersing population  $F_{CFP}$  benefits by getting exclusive access to nutrients by confining  $S_{YFP}$ . As a consequence the population size of  $F_{CFP}$  catches up (day 2) and it finally outcompetes  $S_{YFP}$  (day 3 and 4). Dividing the final competition outcome by regions again unveils spatial segregation of the two populations (figure 3.2f). While fast-growing population  $S_{YFP}$  dominates the inside territory, the fast-dispersing population  $F_{CFP}$  dominates the outside region.

### 3.3 Growth-dispersal trade-offs promote stable coexistence

In nature many species inhabit temporally fluctuating environments in which nutrients become available in discrete patches, e.g. clumps of organic matter in oceans[23, 24], or are refreshed seasonally[42]. These scenarios provide an opportunity for the spatial segregation to occur. Long standing theoretical analyses demonstrated that spatial segregation generated by spatially heterogeneous environments can enable coexistence of multiple species[7]. Here we empirically demonstrated that motile species displaying a growth-dispersal trade-off can spontaneously segregate even in habitats with initially homogeneous nutrient distributions by indirectly interacting through competition for a common nutrient. We employ our numerical model to explore whether spatial segregation can lead to stable coexistence, i.e. the maintenance of both competing populations, in a scenario where dispersal into pristine territory is repeated periodically, and taking the final population ratio of one round as the initial ratio of the following, mimicking seasonal competitions[26, 30, 31] (figure 3.2g).

We fix the parameters of one competition partner (F) and then systematically vary growth rate ( $\mu$ ) and active diffusion coefficient ( $\mathcal{D}$ ) of its competitor (X). We numerically determine whether the two populations can reciprocally invade each other (3.2g, in colour; see Methods for detailed description of classification). We find that for significant regions of parameter space reciprocal invasion, i.e. stable coexistence, can occur (white regions). Spatial segregation is also seen for parameter values not enabling stable coexistence (marker II, depicting  $X = S_{YFP}$ , see supplementary figure 3.11). Thus spatial segregation is not sufficient for stable coexistence. In addition, a sufficiently strong trade-off between growth and dispersal (dispersal rate  $\nu$ ) has to be present.

There are two distinct regions of coexistence in parameter space. The region of coexistence in the lower right is bound by  $\mu_X \approx 1.3\mu_F$  on the left and by  $\mathcal{D}_X \approx 10^{-2} \frac{\text{mm}^2}{\text{h}}$  on the top. The shape of the coexistence region can be rationalised

by the different relations between dispersal rate  $v_X$  and growth ( $\mu_X$ ) and diffusion rate ( $\mathcal{D}_X$ )[43]. The boundary to the left, separating the blue and white region, can be well approximated by a vertical line in parameter space, reflecting that dispersal of slowly diffusing populations is dominated by growth ( $v_X \propto \mu_X$ ). In contrast the boundary on the top, separating the red and white region, displays a slight slope, generated by the dependence of dispersal on growth rate ( $v_X \propto \sqrt{\mu_X \mathcal{D}_X}$ ). Taken together, once X obtains a sufficiently low diffusion coefficient (or fast growth rate) compared to F, a further decrease in motility (or increase in growth) does not affect the occurrence of stable coexistence strongly.

For example two populations of X exhibiting a difference in diffusion coefficient of roughly two orders of magnitude, rendering the latter population practically non-motile, can both coexist with F, illustrating that an additional reduction in motility of X below a threshold has no effect on the occurrence of stable coexistence (compare e.g. marker III and IV in figure 3.2g). For these two competitions both the fixed point ratio and the invasion strength of the two competitors are found to be similar (for definitions see supplementary figure 3.12). Within the second region of coexistence in the upper left of the parameter space, X is the faster dispersing and slower growing population compared to F, even though F exhibits sensing capabilities while X is merely actively diffusing. Hence we can conclude that the ability to sense the local environment does not allow F to escape confinement, but rather only positively influences its dispersal rate above values it would reach by active diffusion and growth alone (see also supplementary figure 3.14 for more details on competitions of populations with and without sensing capabilities). The outline of this region is rather irregular shaped, reflecting the fact that the diffusion coefficient of X has a similar magnitude to the diffusion coefficient of the nutrient ( $\mathcal{D}_{\text{nutrient}} = 1.8 \frac{\text{mm}^2}{\text{h}}$ ), rendering the spatio-temporal competition dynamics complex.

To experimentally verify the predicted stable coexistence in case of sufficiently strong growth-dispersal trade-offs (white regions in figure 3.2g), i.e. population X must at least disperse 30% slower than F while possessing a growth rate advantage of 30% compared to F (coexistence region in the lower left of figure 3.2g), we engineer a slow-dispersing, fast-growing population of *Salmonella typhimurium*,  $S_{\text{st, CFP}}$  (supplementary figure 3.10) as competitor for the fast-dispersing, slow-growing  $F_{\text{YFP}}$  (parameters match approximately figure 3.2g, marker III). Both populations are predicted to successfully invade each other and thus to stably coexist (figure 3.3b, black open circles).

### 3.3 Growth-dispersal trade-offs promote stable coexistence

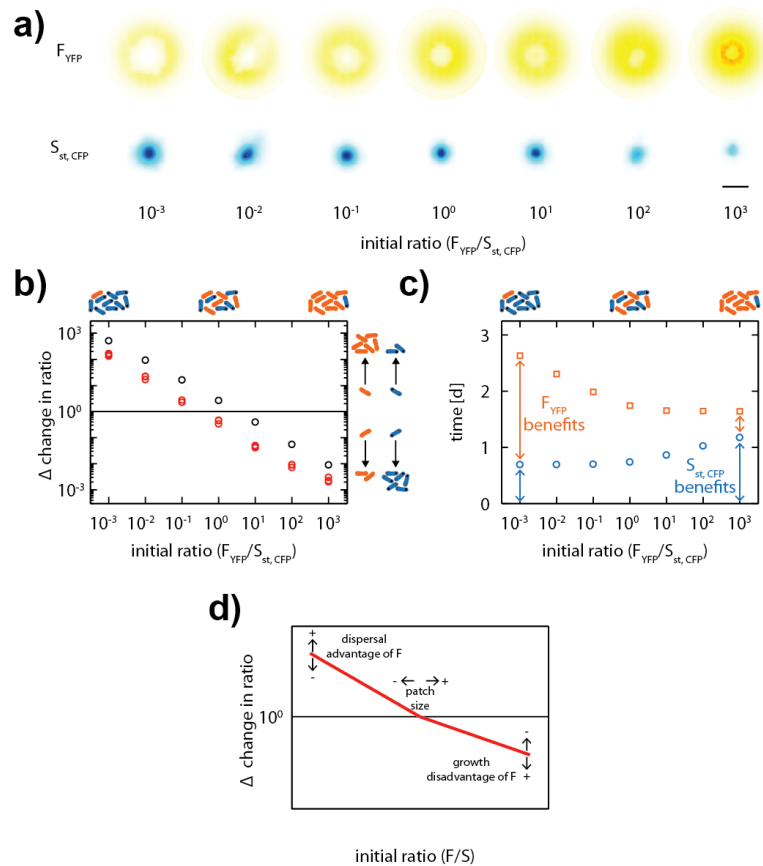


**Figure 3.3: Growth-dispersal trade-offs enable stable coexistence.**

a) Maps of bacterial distributions in fluorescence for various initial population ratios. Scale bar: 10 mm. b) Relative change in population ratio (final ratio over initial ratio) as function of initial population ratio, extracted from fluorescence images (red, open circles) and predicted by theory (black, open circles). c) Model predictions of growth arrest time points of  $S_{st,CFP}$  (blue, open circles) and  $F_{YFP}$  (orange, open squares) as function of initial population ratio. d) Overview of parameters influencing coexistence.

Gathering spatial population distributions of competition outcomes experimentally over a broad range of initial population ratios unveils spatial confinement and segregation of various degrees for all tested initial ratios (figure 3.3a). The faster dispersing population  $F_{YFP}$  always effectively confines  $S_{st,CFP}$ , while the faster growing population  $S_{st,CFP}$  successfully dominates in the centre region. The fraction of space occupied by  $S_{st,CFP}$  increases as function of initial population ratio  $F_{YFP}/S_{st,CFP}$  (figure 3.3a). In contrast the relative change in population ratio at the end of the competition is found to decrease for increasing population ratios (figure 3.3b, red open circles). Hence even though  $S_{st,CFP}$  occupies larger territories when initially a higher abundances,  $F_{YFP}$  is found to successfully invade, i.e. increase over its initial ratio. On the other extreme when  $S_{st,CFP}$  is initially at low abundance, it is also found to successfully invade despite the fact that the size of territory it occupies

is relatively small.

Due to their strong invasive power, final population ratios are identical within one order of magnitude despite the large range of initial ratios, spanning six orders of magnitude. Thus within only one competition round the stable community composition is approximately attained. The ability to invade, i.e. having an advantage over the competitor when at low abundances, known as negative frequency-dependent selection, can be rationalised by noting that the duration of the growth- and dispersal-dominated competition phases varies as a function of initial population ratio (figure 3.3c). The growth-dominated phase is shorter if more fast growers are present initially (initial ratio  $F_{YFP}/S_{CFP}$  smaller than one) as overall local nutrient consumption is higher. Hence the faster growers exhibit only a low increase in abundance and the minority of faster expanders can successfully invade. In contrast, local consumption is slower in the case when few fast growers are present initially (initial ratio  $F_{YFP}/S_{CFP}$  larger than one), turning the growth advantage to their benefit and enabling successful invasion into a population initially dominated by fast dispersers. Taken together these mechanisms explain how a low relative abundance can effectively lead to a competitive advantage for both species. Hence stable coexistence is attained.

## 3.4 Discussion

We found that differential dispersal in combination with competition for a common limiting nutrient is sufficient to generate spontaneous spatial confinement of motile populations even in the absence of preexisting environmental heterogeneities or specific interactions. In addition, when growth-dispersal trade-offs are adequately strong, spatial segregation can lead to stable coexistence of motile species. The different phenotypes are found to harvest region-specific competitive advantages in spatial habitats. While the fast-growing population dominates the region close to the point of inoculation, the fast-dispersing population is found to hold more distant territories. During the initial competition phase dispersal is absent and thus growth dominates the local competition, providing an advantage to the fast growing population. Once the local nutrients are depleted, dispersal takes place, shifting the competitive advantage to the faster disperser. The fast-dispersing population can reach pristine territories first and can hence deplete the nutrients therein, causing its competitor's dispersal and growth to stop. The occurrence of stable coexistence was found to be rather insensitive to changes in growth and dispersal performance beyond minimal trade-off strength, but is certainly influenced by the size of available territory to expand into (figure 3.3d and supplementary figure 3.16). Smaller habitats favour faster growers, while faster dispersers benefit from larger territories. At intermediate habitat sizes stable coexistence is observed. For the populations presented in figure 3.3 we estimate stable coexistence to occur for habitat areas from  $\sim 1 \text{ cm}^2$  to  $\sim 1 \text{ m}^2$ .

Both, spatial confinement and coexistence, are mediated solely through consumption and depletion of a common nutrient and thus can be utilised by primitive

organisms not able to invoke specific interactions, like chemical warfare. In principle growth-dispersal trade-off can be established on the level of prototypic cells not possessing evolved means of active locomotion, as differential passive diffusion, e.g. mediated by differential cell sizes, is sufficient to provide differential dispersal.

Our experimental scenario of a small, point-like inoculation into a homogeneously rich environment reflects a general paradigm of species encountering pristine territories. Windfall of fruits or clumps of organic matter in oceans[24] could represent such territories to micro-organisms like bacteria or nematodes. Growth and dispersal dynamics could be key in exploiting these resources and it has been speculated that observed growth-dispersal trade-offs might explain stable coexistence of natural bacterioplankton populations[21]. The occurrence and stable coexistence of *Escherichia coli* mutants harbouring a growth-dispersal trade-off in mouse guts[44], suggests relevance of our findings to intestinal microbial population dynamics. The gut content is regularly replenished with fresh, uninhabited nutrients and hence forces its inhabitants to invade pristine territory periodically, providing an opportunity for spatial segregation to occur in a seasonal fashion.

More generally, our numerical model, explaining spatial confinement as well as stable coexistence, has a large degree of similarity to existing prey-taxis models employed to successfully describe predator-prey dynamics[45]. It will be interesting to explore whether our findings in the microbial world can be mapped to interactions between species on the macroscale.

## 3.5 Methods

### 3.5.1 Strains and plasmids

*Escherichia coli* K12 strain RP437 [thr leu his metF eda rpsL thi ara lacY xyl tonA tsx] and *Salmonella typhimurium* strain LT2 were employed as background to chromosomal deletions and plasmid transformations (see table 3.1).

Name	Strain	Plasmids
F <sub>YFP</sub>	RP437 (kind gift of H. Berg)	eYFP on pTrc99A empty pKG116
F <sub>CFP</sub>	RP437 (kind gift of H. Berg)	eCFP on pTrc99A empty pKG116
S <sub>YFP</sub>	RP437 $\Delta$ cheY (kind gift of V. Sourjik)	eYFP on pTrc99A cheY D13K Y106W on pKG116
S <sub>CFP</sub>	RP437 $\Delta$ cheY (kind gift of V. Sourjik)	eCFP on pTrc99A cheY D13K Y106W on pKG116
S <sub>st, CFP</sub>	LT2 $\Delta$ cheYZ	eCFP on pTrc99A cheY D13K Y106W on pKG116

**Table 3.1: Strains and plasmids.**

pTrc99A carries a pBr origin of replication, ampicillin antibiotic resistance, and an isopropyl  $\beta$ -D-1-thiogalactopyranoside (IPTG)-inducible induction system. pKG116 carries a pACYC origin of replication, chloramphenicol antibiotic resistance, and a sodium salicylate-inducible induction system.

### 3.5.2 Culture media and growth conditions

For pre-competition growth, bacteria were inoculated from glycerol stocks and grown in 2 ml TB (1% (w/v) tryptone, 0.5% (w/v) NaCl) at 30 °C, 250 rpm, supplemented with antibiotics (100  $\mu$ g ml<sup>-1</sup> ampicillin, 34  $\mu$ g ml<sup>-1</sup> chloramphenicol) for ~ 8 hours. Bacteria were diluted approximately 1:100 into 10 ml minimal medium H1 (50 mM KPO<sub>4</sub>, 7.6 mM (NH<sub>4</sub>)<sub>2</sub>SO<sub>4</sub>, 0.5 mM MgSO<sub>4</sub>, 1.25  $\mu$ M Fe<sub>2</sub>(SO<sub>4</sub>)<sub>3</sub>, 67 mM NaCl, 0.01 % (w/v) Thiamine, pH 7.0) supplemented with 0.1 % (w/v) glycerol, amino acids (1 mM L-histidine, 1 mM L-methionine, 1 mM L-leucine, 1 mM L-threonine and 100  $\mu$ M L-asparagine) and antibiotics, and grown overnight

at 33.5 °C, 250 rpm. Bacteria were diluted approximately 1:100 into 10 ml minimal medium H1 supplemented with glycerol, amino acids, antibiotics and inducers (100 µM isopropyl β-D-1-thiogalactopyranoside, 0.75 µM sodium salicylate) and grown at 33.5 °C, 250 rpm until early-exponential phase ( $OD_{600} \approx 0.1$ ).

For competition growth on soft agar plates, bacterial densities were adjusted to  $OD_{600}$  0.01 and strains were mixed 1:1 or as indicated. Competition medium, minimal medium H1 supplemented with glycerol, amino acids, antibiotics and inducers, was prepared. Soft agar plates were prepared in small petri dishes (Falcon® Easy Grip Petri Dish, polystyrene, 35x10 mm style) by supplementing 4 ml competition medium with 0.26% (w/v) bacto agar (DB). 2 µl strain mixture was inoculated in the centre of a soft agar plate. Soft agar plates were incubated for 4 days at 33.5 °C. A humid environment was mediated by placing a water reservoir close by within the incubation chamber.

For competition in mixed (well-stirred) conditions, bacteria were mixed as for competitions on soft agar plates and grown in 10 ml competition medium at 33.5 °C and 250 rpm for 60 hours, i.e. until saturation was reached. The initial  $OD_{600}$  was adjusted to match the initial ratio of bacteria to nutrients in soft agar plates.

### 3.5.3 Bacterial growth measurements

Bacterial growth was measured in Costar® assay plates (96 well, flat bottom, polystyrene) using a Perkin Elmer Victor™ X3 plate reader. Growth rates were extracted from early-mid exponential phase in competition medium. Mean growth rates were calculated by averaging over several (typically 10-14) wells within one 96-well plate. Error bars in figure 3.1d and supplementary figure 3.10a indicate standard deviations.

### 3.5.4 Fluorescence-based colony counting

At the end of the competition experiments in liquid, cultures were diluted to appropriate densities and spread out on hard agar plates (competition medium supplemented with 1.5% agar). Similarly soft agar plate competitions were first dissolved by applying heat (8 minutes at 40 °C) followed by manual shaking and then diluted and spread out. Hard agar plates were incubated for 24-48 hours at 37 °C and subsequently imaged in grid fashion using a Nikon 2x/0.10 Plan Apo objective. Focus was adjusted manually in brightfield onto the colonies. Fluorescence was imaged in YFP and CFP channels while exposure time was kept fixed for each fluorescence channel. Images were not corrected in any way. Colonies were counted manually with the help of ImageJ[46]. Population ratios  $pr$  were obtained as ratios of colony counts in the respective fluorescence channels. Errors in figure 3.1e-f express as predicted standard deviation over population ratio  $\left(\frac{\sigma_{pr}}{pr}\right)$ .

$$N_x = c \cdot N \quad (3.1)$$

$$N_y = (1 - c) \cdot N \quad (3.2)$$

$$pr = \frac{N_x}{N_y} \quad (3.3)$$

$$\sigma_{pr} = \left| \frac{N_x}{N_y} \right| \sqrt{\left( \frac{\sigma_{N_x}}{N_x} \right)^2 + \left( \frac{\sigma_{N_y}}{N_y} \right)^2} \quad (3.4)$$

$$\frac{\sigma_{pr}}{pr} = \sqrt{\frac{1}{c \cdot (1 - c) \cdot N}} \quad (3.5)$$

$N_x$  and  $N_y$  denote colony counts of populations x and y, respectively, and  $N$  the total colony count.  $c \in [0,1]$ .

### 3.5.5 Microscopy

A Nikon Eclipse Ti inverted microscope was used with a Nikon 4x/0.13 Plan Fluor objective, a Hamamatsu Orca Flash 4.0 CMOS camera (2024x2024 pixel, pixel size 6.5  $\mu\text{m}$  x 6.5  $\mu\text{m}$ ), a Lumencor® Sola light engine LED and a motorized Märzhäuser scanning stage equipped with a custom petri dish holder to image spatial distributions of bacterial populations on soft agar plates. The microscope body and the stage were encased by a custom-built incubation chamber equipped with temperature control. The microscope was controlled via custom-written scripts through MicroManager[47]. Plates were scanned in a grid fashion (11x11 images per plate) while images were collected at a focus approximately 1.5 mm above the plate's bottom. Exposure times were automatically adjusted for each grid position to stay within the dynamic range of the camera. Images were binned 4x4 pixels by MicroManager.

### 3.5.6 Image and data analysis

Images of soft agar plates were corrected for camera offset and inhomogeneous fluorescence illumination by subtracting an experimentally obtained camera offset and dividing by measured illumination patterns. Illumination patterns were obtained for each fluorescence channel individually by imaging gels containing spatially homogeneous bacterial distributions. Subsequently image intensities were rescaled by exposure time. Images were assembled into montages and resized by  $\frac{1}{10}$ . Fluorescence intensities ( $I$ ) were converted into proxies for bacterial densities ( $D$ ).

$$I_{\text{CFP}} = A_{\text{CFP strain}} \cdot D_{\text{CFP strain}} + B_{\text{CFP}} + C_{\text{YFP to CFP}} \cdot A_{\text{YFP strain}} \cdot D_{\text{YFP strain}} \quad (3.6)$$

$$I_{\text{YFP}} = A_{\text{YFP strain}} \cdot D_{\text{YFP strain}} + B_{\text{YFP}} + C_{\text{CFP to YFP}} \cdot A_{\text{CFP strain}} \cdot D_{\text{CFP strain}} \quad (3.7)$$



Proxies obtained from fluorescence images were found to overestimate the size of confined populations compared to fluorescence-based colony counting, but deviations were found to be within a factor of 6. This discrepancy does not affect our general findings. Slopes  $A$  and background intensities  $B$  were obtained by linear fitting of equations 3.6 and 3.7 to mean fluorescence intensities extracted from soft agar plates containing known, spatially homogeneous bacterial densities of single, labelled strains. Crosstalk coefficients  $C$  were estimated from correlations of fluorescence intensities of both imaging channels in soft agar gels containing a single, labelled strain (supplementary figure 3.13). Population sizes and radial density profiles were extracted from inside the petri dishes. Petri dish location and colony centre were selected manually. Population sizes are maximum normalised within each competition individually. Radial bacterial densities were arbitrarily normalised by the maximum bacterial radial density reached by  $S_{CFP}$  in soft agar gels when grown without competitor. Ratios were computed as ratio of population sizes of the competing populations. Dispersal was followed by tracking the population fronts in radial density profiles over time after leaving the region of inoculation. Dispersal rate,  $\nu$ , is extracted by fitting a first order polynomial to the colony dispersal dynamics. The mean value over different threshold value definitions of the colony front position (0.0125, 0.015, 0.0175, 0.02, 0.0225 and 0.025 in normalised units) is reported. Error bars denote the corresponding standard deviations.

### 3.5.7 Numerical analysis of competitions on soft agar plates

We compute the time evolution of spatial density profiles of motile populations,  $p_x$  and  $p_y$ , by numerically evaluating a set of modified Keller-Segel equation[40] with a Monod growth term[32] coupled to a diffusing nutrient,  $n$ . We express the equations in polar coordinates and assume radial symmetry. Equations were numerically solved using Matlab R2013b (The MathWorks Inc., Natick, MA, 2000).

$$\frac{\partial p_x}{\partial t} = r^{-1} \underbrace{\frac{\partial}{\partial r} \left( r \frac{n}{K+n} \left( \mathcal{D}_x \frac{\partial p_x}{\partial r} - \chi_x p_x \frac{\partial n}{\partial r} \right) \right)}_{\text{active motility}} + \underbrace{\ln(2) \frac{n}{K+n} \mu_x p_x}_{\text{growth}} \quad (3.8)$$

$$\frac{\partial p_y}{\partial t} = r^{-1} \underbrace{\frac{\partial}{\partial r} \left( r \frac{n}{K+n} \left( \mathcal{D}_y \frac{\partial p_y}{\partial r} - \chi_y p_y \frac{\partial n}{\partial r} \right) \right)}_{\text{active motility}} + \underbrace{\ln(2) \frac{n}{K+n} \mu_y p_y}_{\text{growth}} \quad (3.9)$$

$$\frac{\partial n}{\partial t} = r^{-1} \underbrace{\frac{\partial}{\partial r} \left( r \mathcal{D}_n \frac{\partial n}{\partial r} \right)}_{\text{diffusion}} - \underbrace{\ln(2) \frac{n}{K+n} (\mu_x p_x + \mu_y p_y)}_{\text{consumption}} \quad (3.10)$$

We assume the Monod coefficient  $K$  to be  $10^{-3}$  a.u., in the range of reported values[48], i.e. three orders of magnitude below typical nutrient concentrations. The nutrient's diffusion coefficient,  $\mathcal{D}_n$ , is set to  $1.8 \text{ mm}^2 \text{ h}^{-1}$ , a value typically used

for small molecules in aqueous solutions[49]. Growth rates,  $\mu$ , are taken from figure 3.1 and supplementary figure 3.10. The active diffusion coefficients,  $\mathcal{D}$ , were tuned to match the observed dispersal rates of  $S_{YFP}$ ,  $S_{CFP}$  and  $S_{st, CFP}$  when grown on soft agar plates without competitor. Simulated colony fronts were tracked at a threshold of 0.0125 a.u. comparable to the threshold used on the experimental data.  $\chi$ , the chemotactic sensitivity coefficient, is zero for these populations since they do not possess sensing capabilities. For  $F_{YFP}$  and  $F_{CFP}$  we assumed  $\mathcal{D}$  to match the diffusion coefficient of  $S_{YFP}$ . Subsequently  $\chi$  is tuned to match their observed dispersal rates when grown on soft agar plates without a competitor. For an overview of all population-specific parameter values see table 3.2.

Population	$\mu$ [db/h]	$\mathcal{D}$ [mm <sup>2</sup> /h]	$\chi$ [mm <sup>2</sup> /(a.u. h)]
$F_{YFP}$	0.423	0.02	0.875
$F_{CFP}$	0.404	0.02	0.875
$S_{YFP}$	0.470	0.02	0.0
$S_{CFP}$	0.462	0.01	0.0
$S_{st, CFP}$	0.834	0.01	0.0

**Table 3.2: Simulation parameters.**

The initial nutrient profiles is assumed to be flat ( $n(t = 0) = 1$  a.u. for all  $r$ ), while the initial bacterial populations are modelled as a plateau of height  $p_{initial}$  and radius  $r_{plateau}$  ( $r_{plateau} = 1$  mm) and an adjacent exponentially decaying tail,  $p_{initial} \exp[-\lambda(r - r_{plateau})]$ . We assume a sharp boundary at the edge of the inoculum since the initial bacterial population is inoculated via pipetting and set  $\lambda$  to  $10 \text{ mm}^{-1}$ , on the order of several tens of a single bacterium's length.  $p_{initial, x} + p_{initial, y}$  is set to  $10^{-3}$  a.u. to match the experimental initial densities employed in competitions on soft agar plates. The habitat radius is set to 17.5 mm, matching the radius of the petri dishes used in experiments, if not noted otherwise.

We modified the dispersal term in the Keller-Segel equations with a Monod-like factor ( $\frac{n}{K+n}$ ) to account for energy dependence of the active movement of the bacterial populations. The final population ratio does not change significantly when this factor is omitted, while the final spatial population profile changes as profiles flatten out due to active diffusion. We did not observe flattening out of bacterial profiles experimentally.

Final community structures shown in figure 3.2 and supplementary figure 3.14 are obtained by propagating competition simulations for initial population ratios

of  $10^{-5}$  and  $10^5$  (X over F) for 7 or 28 days. Final population ratios are extracted from the last time point. In all cases the total amount of nutrient had dropped to less than a  $10^{-6}$ th of its initial amount, i.e. the nutrient was depleted. Final community structures are then classified as follows:

- F excludes X: final ratio decreased for both initial ratios.
- X excludes F: final ratio increased for both initial ratios.
- stable coexistence: final ratio increased for initial ratio of  $10^{-5}$  and decreased for initial ratio of  $10^5$ .
- unstable coexistence: at least for one of the initial ratios the final ratio did not change within a specified tolerance ( $\log_{10} \left( \frac{\text{final ratio}}{\text{initial ratio}} \right) \leq 10^{-5}$ ).

Final community structures shown in supplementary figure 3.16 are estimated accordingly.

Simulation results shown in box 3.1 are performed in one dimensional Cartesian space instead of polar coordinates.

### 3 Microbial diversity promoted by spontaneous spatial segregation

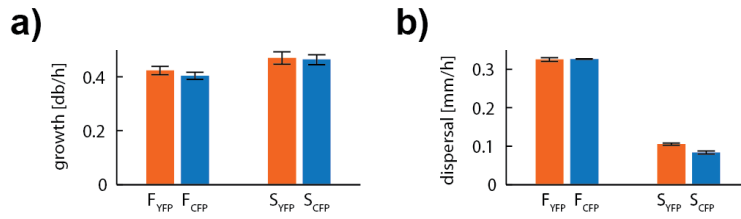


**Figure 3.4: Growth and dispersal.** Growth and dispersal. a) Growth rates are determined in early-mid exponential phase (error bars denote standard deviations of 12-14 replicas). b) Dispersal rates are obtained by tracking colony fronts over time (error bars denote standard deviations over different colony front thresholds).

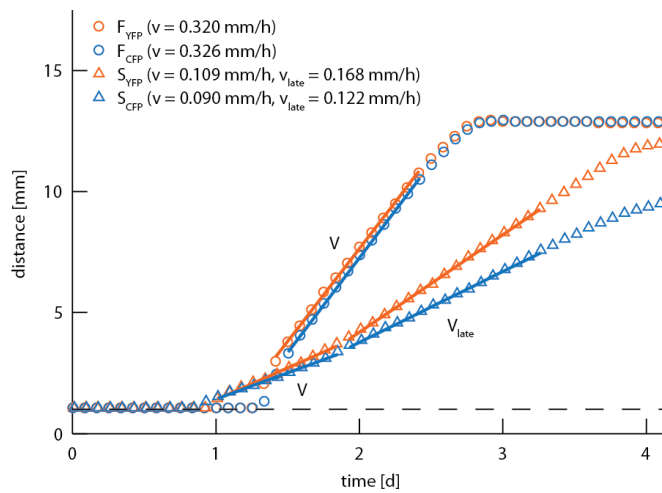


**Figure 3.5: Dispersal dynamics of  $F_{YFP}$ ,  $F_{CFP}$ ,  $S_{YFP}$  and  $S_{CFP}$ .** Population front positions (threshold 0.0125 in normalised units) as function of time used to extract dispersal rates ( $v$ ).  $v_{late}$  is employed instead of  $v$  for  $S_{YFP}$  and  $S_{CFP}$  in the model predictions shown in figure 3.2a-c.

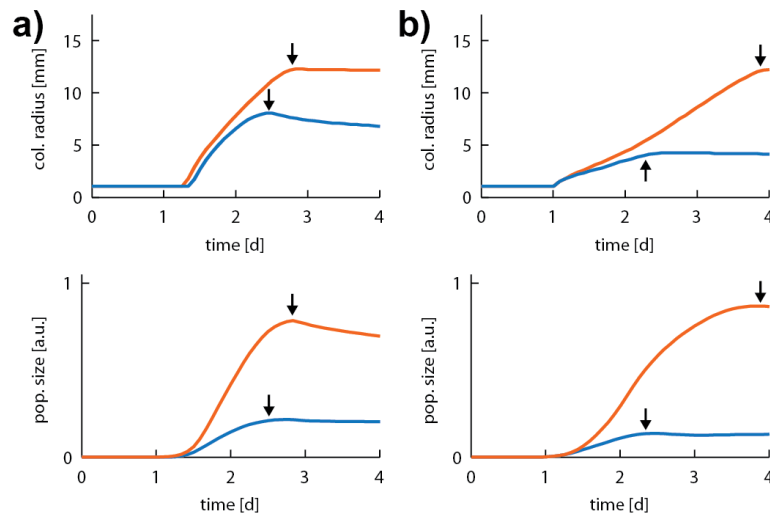


**Figure 3.6: Competition dynamics:  $F_{YFP}$  vs  $F_{CFP}$  and  $S_{YFP}$  vs  $S_{CFP}$ .** a)  $F_{YFP}$  vs  $F_{CFP}$ : dispersal of  $F_{YFP}$  (orange) and  $F_{CFP}$  (blue) cease approximately simultaneously. Halting of population size increase coincides with ceasing of dispersal. b)  $S_{YFP}$  vs  $S_{CFP}$ : dispersal of  $S_{CFP}$  (blue) ceases earlier than dispersal of  $S_{YFP}$  (orange). The same holds true for the halting of their respective population sizes. Arrows indicate approximate time points of dispersal and growth arrest.

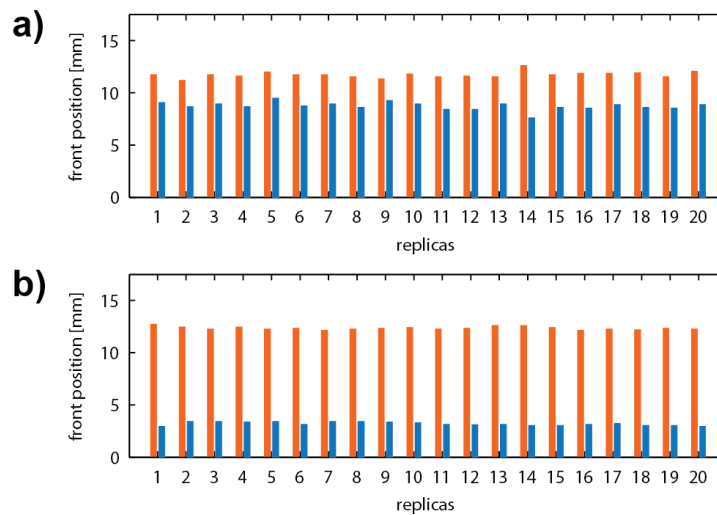


**Figure 3.7: Dispersed distance:  $F_{YFP}$  vs  $F_{CFP}$  and  $S_{YFP}$  vs  $S_{CFP}$ .** a)  $F_{YFP}$  vs  $F_{CFP}$ : only minor difference in dispersed distance of  $F_{YFP}$  (orange) and  $F_{CFP}$  (blue) after 4.5 days of competition on soft agar plates. b)  $S_{YFP}$  vs  $S_{CFP}$ : clear difference in dispersed distance of  $S_{YFP}$  (orange) and  $S_{CFP}$  (blue) after 4.5 days of competition on soft agar plates.

### 3 Microbial diversity promoted by spontaneous spatial segregation

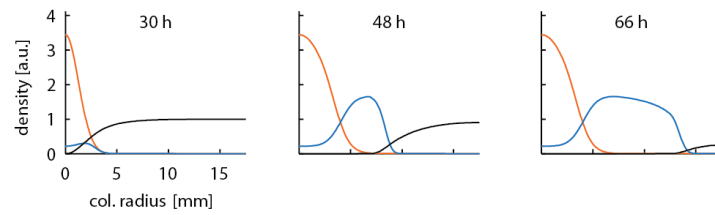


**Figure 3.8: Spatial confinement is caused by local nutrient depletion.** Model predictions of spatial segregation. Radial profiles of  $S_{YFP}$  (orange),  $F_{CFP}$  (blue) and nutrient (black). Spatial confinement of  $S_{YFP}$  is caused by local nutrient depletion. The front of  $S_{YFP}$  loses contact to nutrients after approximately 48 hours.

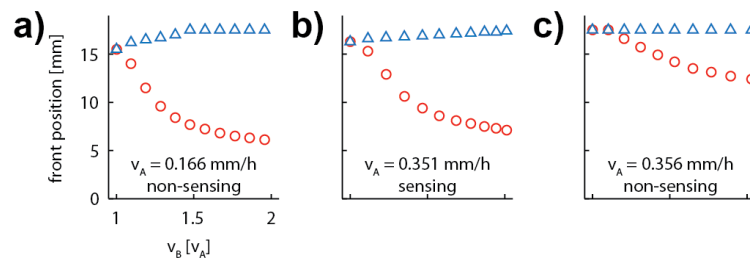


**Figure 3.9: Spatial confinement is determined by differences in dispersal rate independently of presence or absence of sensing capabilities.** a-c) Model predictions of front positions after 4 days as function of dispersal rate for two motile populations, A (red) and B (blue), in competition. Sensing abilities of both populations are identical and are marked within the panels.

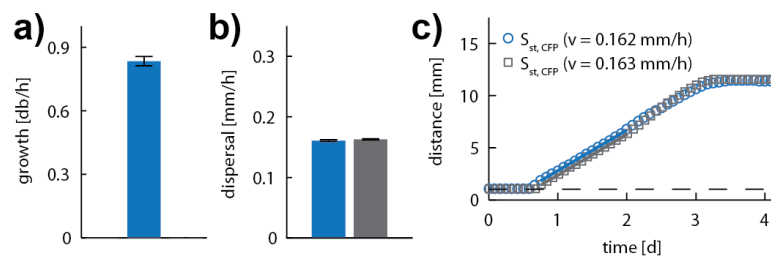


**Figure 3.10: Growth and dispersal of the slow-dispersing, fast-growing *Salmonella* population  $S_{st,CFP}$ .** a) Growth rate was determined in early-mid exponential phase (error bar denotes standard deviation over 27 replicas). b-c) Dispersal rates were obtained by tracking colony fronts over time (error bars denote standard deviations over different colony front thresholds). Colony front threshold in c: 0.0125 in normalised units. Blue and grey depict two individual replicas.

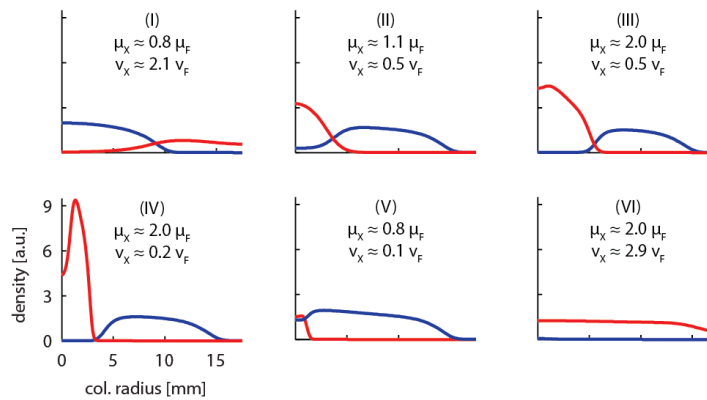


**Figure 3.11: Colony profiles.** Model predictions of colony profiles after 4 days. Initial population ratio 1:1. I-IV depict spatial segregation, while V and VI do not. I-VI as defined in figure 3.2g. F (blue) and X (red).

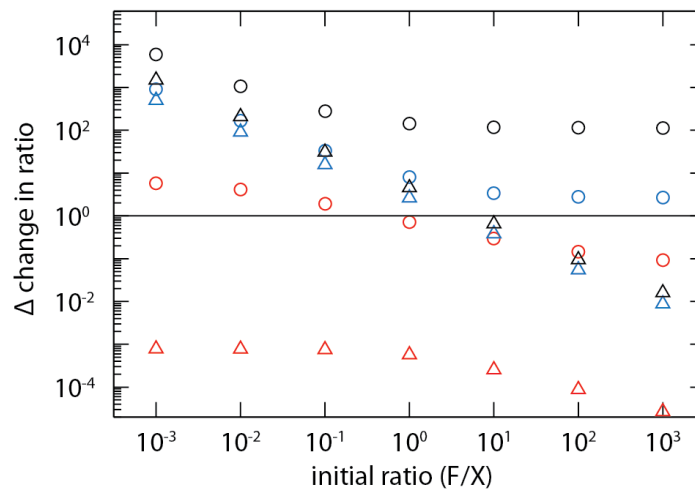


**Figure 3.12: Invasion and stable coexistence.** Model predictions for relative changes in population ratio for the six parameter sets highlighted in figure 3.2g. I: red circles, II: blue circles, III: blue triangles, IV: black triangles, V: black circles and VI: red triangles. I, III and IV depict reciprocal invasion of both populations and stable coexistence, while II, V and VI do not. Fixed point ratios are defined by the intersection with the black line marking a relative change in ratio equal to 1, indicative of no change in ratio. Invasion strength, i.e. the speed with which the system approaches the fixed point, is directly related to the slopes of the curves. Steeper curves indicate stronger invasion.

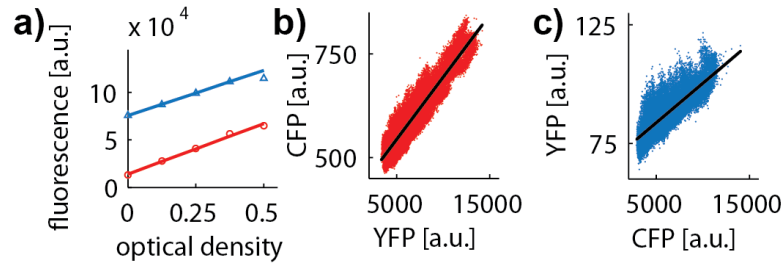


**Figure 3.13: Fluorescence-bacterial density conversion.** a) Fluorescence as function of optical density at 600 nm for CFP (blue triangles) and YFP (red circles), and their respective linear fits (solid lines). Last point for CFP data was excluded while fitting. b-c) Crosstalk of fluorescent channels obtained from populations carrying only one type of fluorophore. Black lines show linear fits.

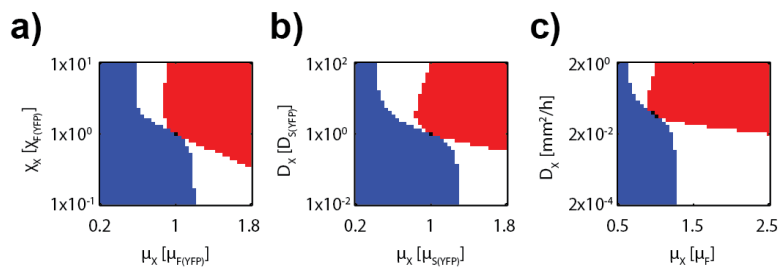


**Figure 3.14: Coexistence can occur when a sufficiently strong growth-dispersal trade-off is present independent of presence or absence of sensing capabilities.** Final community structures (dark blue:  $F_{YFP}/S_{YFP}/F$  excludes X, red: X excludes  $F_{YFP}/S_{YFP}/F$ , white: stable coexistence, black: unstable coexistence). a) Both populations have sensing capabilities. b) Both populations have no sensing capabilities). c) F can sense, while X cannot.



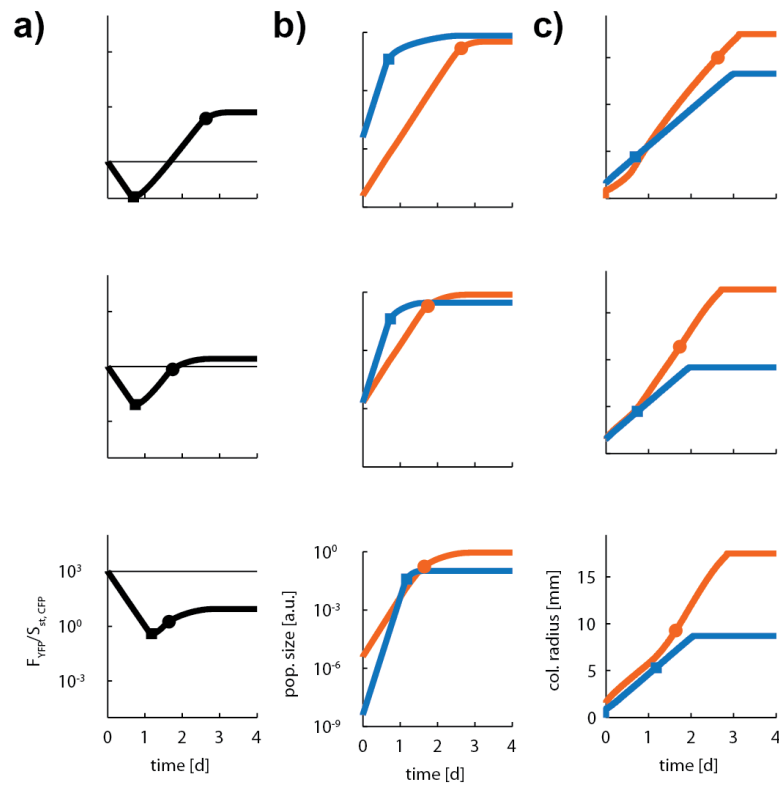


**Figure 3.15: Simulated competition dynamics,  $F_{YFP}$  vs  $S_{St,CFP}$ , for different initial population ratios.** a) Population ratio as function of time. b) Total population sizes of  $F_{YFP}$  (orange) and  $S_{St,CFP}$  (blue) as function of time. c) Dispersal dynamics of  $F_{YFP}$  (orange) and  $S_{St,CFP}$  (blue) as function of time obtained by tracking a threshold value of  $10^{-6}$  a.u. in the radial colony profile. Filled, blue square (filled, orange circle) mark time point when population growth of  $F_{YFP}$  ( $S_{St,CFP}$ ) decreases below 50% of its initial growth rate, i.e. growth arrest as reported in figure 3.3c.

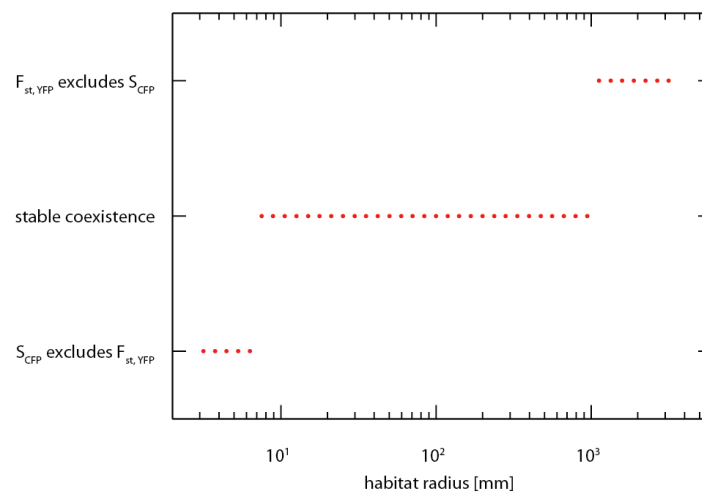


**Figure 3.16: Estimated final community structures as function of habitat size.** Occurrence of stable coexistence depends on habitat size for a fixed growth-dispersal trade-off ( $F_{YFP}$  vs  $S_{st, CFP}$ ). Final community structures are estimated by dividing the (circular) habitat in two distinct areas. An inner one with radius 6.9 mm (confinement radius obtained from competition model, habitat radius = 17.5 mm, population ratio 1:1) where both populations grow exponentially and compete for nutrients, and an complementary outer one, which is solely inhabited by  $F_{YFP}$ , the faster dispersing population. Total initial population size is assumed to be  $10^5$  individuals, matching experimental conditions. Final community structures are classified as described in Methods.

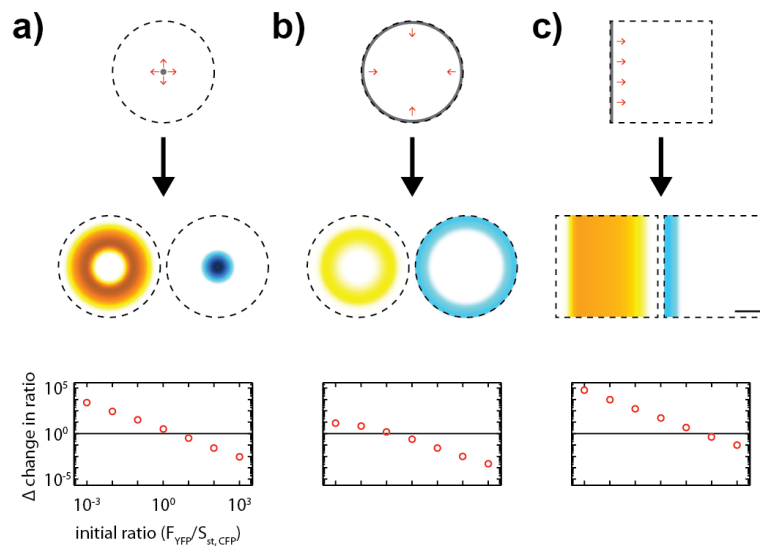


**Figure 3.17: Spatial segregation and stable coexistence can occur in various geometries.** Illustration of initial bacterial distributions (top), simulated competition outcomes of  $F_{YFP}$  (in yellow) vs  $S_{st,CFP}$  (in blue) at initial ratio 1:1 (middle) and simulated relative changes in ratio (final ratio / initial ratio) as function of initial ratio (bottom) for a circular geometry with central inoculation (a), a circular geometry with boundary inoculation (b) and a squared geometry with line inoculation (c). Nutrients are initially spatially homogeneously distributed in all cases and total bacterial densities are set to  $10^{-3}$  a.u. within the regions of inoculation (grey areas).  $F_{YFP}$  and  $S_{st,CFP}$  are found to stably coexist for all tested geometries. Dashed lines mark habitat boundaries. Scale bar: 10 mm.

### 3 Microbial diversity promoted by spontaneous spatial segregation

---

## References

- [1] C. R. Darwin, *On the Origin of Species by Means of Natural Selection, or the Preservation of Favoured Races in the Struggle for Life*, London: John Murray, 1859.
- [2] A. J. Lotka, *Analytical note on certain rhythmic relations in organic systems*, Proceedings of the National Academy of Sciences of the United States of America **6**, 410 (1920).
- [3] V. Volterra, *Variations and fluctuations of the number of individuals in animal species living together*, J. Cons. Int. Explor. Mer **3**, 3 (1928).
- [4] R. MacArthur and R. Levins, *Competition, habitat selection, and character displacement in a patchy environment*, Proceedings of the National Academy of Sciences of the United States of America **51**, 1207 (1964).
- [5] S. A. Levin, *Community equilibria and stability, and an extension of the competitive exclusion principle*, American Naturalist , 413 (1970).
- [6] B. R. Levin, *Coexistence of two asexual strains on a single resource*, Science **175**, 1272 (1972).
- [7] N. Shigesada, K. Kawasaki, and E. Teramoto, *Spatial segregation of interacting species*, Journal of Theoretical Biology **79**, 83 (1979).
- [8] R. A. Armstrong and R. McGehee, *Competitive exclusion*, American Naturalist , 151 (1980).
- [9] B. J. Bohannan, B. Kerr, C. M. Jessup, J. B. Hughes, and G. Sandvik, *Trade-offs and coexistence in microbial microcosms*, Antonie van Leeuwenhoek **81**, 107 (2002).
- [10] K. L. Yurewicz, *A growth/mortality trade-off in larval salamanders and the coexistence of intraguild predators and prey*, Oecologia **138**, 102 (2004).
- [11] A. L. Angert, T. E. Huxman, P. Chesson, and D. L. Venable, *Functional tradeoffs determine species coexistence via the storage effect*, Proceedings of the National Academy of Sciences **106**, 11641 (2009).
- [12] Y. Onoda, J. B. Saluñga, K. Akutsu, S.-i. Aiba, T. Yahara, and N. P. Anten, *Trade-off between light interception efficiency and light use efficiency: implications for species coexistence in one-sided light competition*, Journal of Ecology **102**, 167 (2014).
- [13] G. E. Hutchinson, *Copepodology for the Onithologist*, Ecology , 571 (1951).
- [14] R. Levins and D. Culver, *Regional coexistence of species and competition between rare species*, Proceedings of the National Academy of Sciences **68**, 1246 (1971).
- [15] H. S. Horn and R. H. Mac Arthur, *Competition among fugitive species in a harlequin environment*, Ecology , 749 (1972).
- [16] R. A. Armstrong, *Fugitive species: experiments with fungi and some theoretical considerations*, Ecology , 953 (1976).
- [17] A. Hastings, *Disturbance, coexistence, history, and competition for space*, Theoretical population biology **18**, 363 (1980).
- [18] I. Hanski and E. Ranta, *Coexistence in a patchy environment: three species of Daphnia in rock pools*, The Journal of Animal Ecology , 263 (1983).
- [19] A. Shmida and S. Ellner, *Coexistence of plant species with similar niches*, Vegetatio **58**, 29 (1984).
- [20] D. Tilman, *Competition and biodiversity in spatially structured habitats*, Ecology **75**, 2 (1994).

## REFERENCES

---

- [21] Y. Yawata, O. X. Cordero, F. Menolascina, J.-H. Hehemann, M. F. Polz, and R. Stocker, *Competition–dispersal tradeoff ecologically differentiates recently speciated marine bacterioplankton populations*, *Proceedings of the National Academy of Sciences* **111**, 5622 (2014).
- [22] A. B. Duthie, K. C. Abbott, and J. D. Nason, *Trade-Offs and Coexistence in Fluctuating Environments: Evidence for a Key Dispersal-Fecundity Trade-Off in Five Nonpollinating Fig Wasps*, *The American Naturalist* **186**, 151 (2015).
- [23] J. T. Lehman and D. Scavia, *Microscale patchiness of nutrients in plankton communities*, *Science* **216**, 729 (1982).
- [24] F. Azam and F. Malfatti, *Microbial structuring of marine ecosystems*, *Nature Reviews Microbiology* **5**, 782 (2007).
- [25] R. Durrett and S. Levin, *Spatial aspects of interspecific competition*, *Theoretical population biology* **53**, 30 (1998).
- [26] B. Kerr, M. A. Riley, M. W. Feldman, and B. J. Bohannan, *Local dispersal promotes biodiversity in a real-life game of rock–paper–scissors*, *Nature* **418**, 171 (2002).
- [27] T. L. Czárán, R. F. Hoekstra, and L. Pagie, *Chemical warfare between microbes promotes biodiversity*, *Proceedings of the National Academy of Sciences* **99**, 786 (2002).
- [28] T. Reichenbach, M. Mobilia, and E. Frey, *Mobility promotes and jeopardizes biodiversity in rock–paper–scissors games*, *Nature* **448**, 1046 (2007).
- [29] E. D. Kelsic, J. Zhao, K. Vetsigian, and R. Kishony, *Counteraction of antibiotic production and degradation stabilizes microbial communities*, *Nature* (2015).
- [30] R. C. MacLean and I. Gudelj, *Resource competition and social conflict in experimental populations of yeast*, *Nature* **441**, 498 (2006).
- [31] J. Gore, H. Youk, and A. Van Oudenaarden, *Snowdrift game dynamics and facultative cheating in yeast*, *Nature* **459**, 253 (2009).
- [32] J. Monod, *The Growth of Bacterial Cultures*, *Annual Reviews in Microbiology* **3**, 371 (1949).
- [33] M. Schaechter, O. Maaløe, and N. Kjeldgaard, *Dependency on medium and temperature of cell size and chemical composition during balanced growth of *Salmonella typhimurium**, *Journal of General Microbiology* **19**, 592 (1958).
- [34] S. Klumpp, Z. Zhang, and T. Hwa, *Growth rate-dependent global effects on gene expression in bacteria*, *Cell* **139**, 1366 (2009).
- [35] H. C. Berg, *Motile behavior of bacteria*, *Physics Today* **53**, 24 (2000).
- [36] J. Gray and H. W. Lissmann, *The locomotion of nematodes*, *Journal of Experimental Biology* **41**, 135 (1964).
- [37] R. A. Fisher, *The wave of advance of advantageous genes*, *Annals of Eugenics* **7**, 355 (1937).
- [38] V. Tikhomirov, *A study of the diffusion equation with increase in the amount of substance, and its application to a biological problem*, in *Selected works of AN Kolmogorov*, pages 242–270, Springer, 1991.
- [39] O. Hallatschek, P. Hersen, S. Ramanathan, and D. R. Nelson, *Genetic drift at expanding frontiers promotes gene segregation*, *Proceedings of the National Academy of Sciences* **104**, 19926 (2007).
- [40] E. F. Keller and L. A. Segel, *Model for chemotaxis*, *Journal of theoretical biology* **30**, 225 (1971).

- 
- [41] J. Liu, A. Prindle, J. Humphries, M. Gabalda-Sagarra, M. Asally, D. L. Dong-yeon, S. Ly, J. Garcia-Ojalvo, and G. M. Süel, *Metabolic co-dependence gives rise to collective oscillations within biofilms*, *Nature* **523**, 550 (2015).
- [42] K. Stephens, R. Sheldon, and T. Parsons, *Seasonal variations in the availability of food for benthos in a coastal environment*, *Ecology* , 852 (1967).
- [43] W. van Saarloos, *Front propagation into unstable states*, *Physics reports* **386**, 29 (2003).
- [44] M. De Paepe et al., *Trade-off between bile resistance and nutritional competence drives *Escherichia coli* diversification in the mouse gut*, *PLoS Genet* **7**, e1002107 (2011).
- [45] P. Kareiva and G. Odell, *Swarms of predators exhibit "preytaxis" if individual predators use area-restricted search*, *American Naturalist* , 233 (1987).
- [46] C. A. Schneider, W. S. Rasband, and K. W. Eliceiri, *NIH Image to ImageJ: 25 years of image analysis*, *Nature methods* **9**, 671 (2012).
- [47] A. Edelstein, N. Amodaj, K. Hoover, R. Vale, and N. Stuurman, *Computer control of microscopes using  $\mu$ Manager*, *Current protocols in molecular biology* , 14 (2010).
- [48] H. Senn, U. Lendenmann, M. Snozzi, G. Hamer, and T. Egli, *The growth of *Escherichia coli* in glucose-limited chemostat cultures: a re-examination of the kinetics*, *Biochimica et Biophysica Acta (BBA)-General Subjects* **1201**, 424 (1994).
- [49] J. R. Hazel and B. D. Sidell, *A method for the determination of diffusion coefficients for small molecules in aqueous solution*, *Analytical biochemistry* **166**, 335 (1987).

## REFERENCES

---



# 4

---

## Growth in spatial habitats

When inoculated from a point, motile populations can exhibit spatial segregation (chapter 3). Here we investigate the effect of initial conditions on growth and competition dynamics in spatial habitats. We systematically vary total initial population size, initial population ratio and the initial spatial profile and determine the resulting effects on spatial segregation. We focus on  $S_{YFP}$  and  $F_{YFP}/F_{CFP}$  since the populations are derived from an identical genetic background.

### 4.1 Effects of initial population size

Variations in total initial population size, for initial  $S_{YFP}/F_{CFP}$  population ratios of 1:1, are found to not substantially influence the final spatial profile of population densities (figure 4.1a). The relative change in population ratio is also observed to be largely independent of the initial population size (figure 4.1b). However, smaller initial population sizes result in a prolonged maintenance of growth of the confined population,  $S_{YFP}$ , as  $S_{YFP}$  reaches its maximal population size later for smaller total initial population sizes than for larger ones (figure 4.1c). Inspection of time lapse movies reveals that spatial confinement is delayed for smaller total initial population sizes relative to the time point of spatial confinement observed for larger total initial population sizes (data not shown). Nevertheless the size of territory occupied by  $S_{YFP}$  remains unchanged as the tails of its radial profiles collapse on top of each other (figure 4.1d). Theory predicts a slight dependence of the competition outcome on initial population size (approximately a factor of 2 over the scanned regime), which we are not able to resolve experimentally.

---

The work presented in this chapter is a collaborative effort of Sebastian Gude, Katja M. Taute, Thomas S. Shimizu, and Sander J. Tans

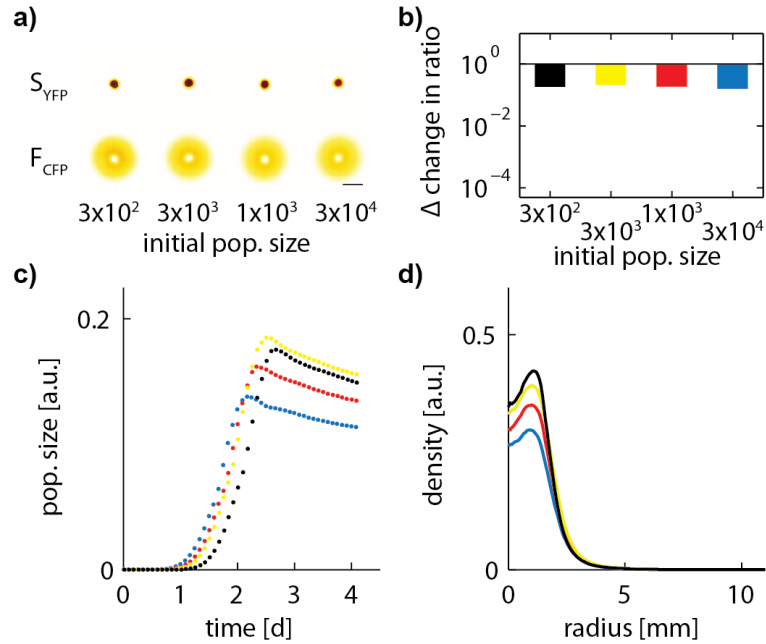


**Figure 4.1: Effects of initial population size.** a) Spatial profiles of population densities after 4 days for various initial population sizes. Colour scale: white-yellow-red-black (low to high densities). Scale bar: 10 mm. b) Relative change in community composition ( $(S_{YFP, final}/F_{CFP, final})/(S_{YFP, initial}/F_{CFP, initial})$ ) after 4 days. c) Population sizes and d) radial density profiles of  $S_{YFP}$  after 4 days. Colours as defined in b.

## 4.2 Effects of initial population ratio

Changes in initial population ratio ( $S_{YFP}/F_{CFP}$ ) at fixed initial population size have more profound consequences (figure 4.2). We bias the initial population ratio to favour the confined population,  $S_{YFP}$ , i.e. towards ratios larger than one. Spatial segregation can occur for initial population ratios up to  $10^4$ , corresponding to an initial population size of  $F_{CFP}$  on the order of just 10 individuals in a total population of  $10^5$  individuals (figure 4.2a). Visual inspection of spatial profiles of population densities reveals a clear link between initial population ratio and the size of territory occupied by the confined population,  $S_{YFP}$ . More biased initial population ratios result in larger areas inhabited by  $S_{YFP}$ . With the aid of extracted radial profiles we can confirm this trend (figure 4.2d). Inspection of time lapse movies reveals a delayed occurrence of confinement and segregation (data not shown), which we interpret as a consequence of the inability of  $F_{CFP}$  to confine  $S_{YFP}$  when it has not yet reached sufficient densities. During this period both populations are able to spread and grow, though  $F_{CFP}$  can employ sensing to locate nutrients more efficiently than  $S_{YFP}$ , elevating its effective growth rate. Overall growth of  $S_{YFP}$  stops later for more biased population ratios (figure 4.2c), in agreement with a delayed occurrence of spatial segregation. The relative change in population ratio shows a strong dependence

on initial population ratio, reflecting the growth advantage obtained by  $F_{CFP}$  by means of confining  $S_{YFP}$  (figure 4.2b). The relative increase of  $S_{YFP}$  over  $F_{CFP}$  rises strongly for more biased initial ratios, indicating frequency-dependent selection.

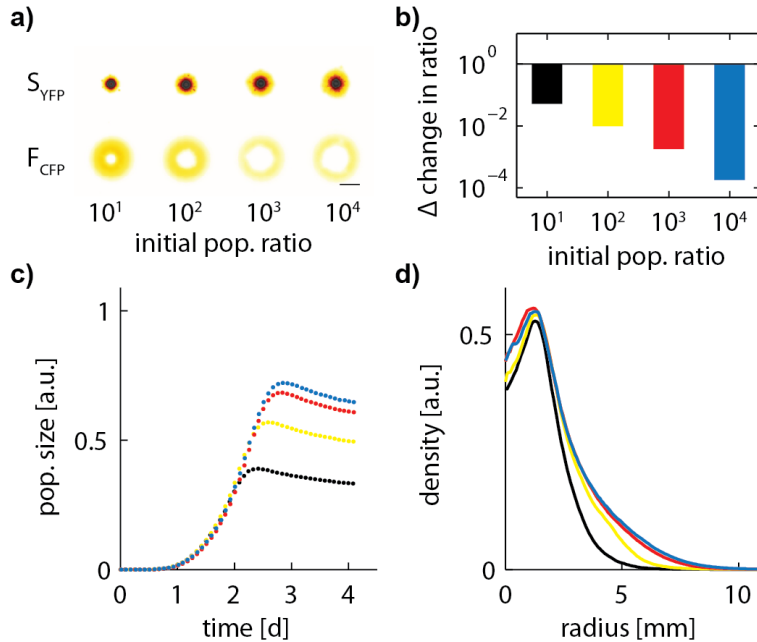


**Figure 4.2: Effects of initial population ratio.** a) Spatial profiles of population densities after 4 days of competition for various initial population ratios. Colour scale: white-yellow-red-black (low to high densities). Scale bar: 10 mm. b) Relative change in community composition ( $S_{YFP_{final}}/F_{CFP_{final}}/(S_{YFP_{initial}}/F_{CFP_{initial}})$ ) after 4 days. c) Population sizes and d) radial density profiles of  $S_{YFP}$  after 4 days. Colours as defined in b.

Frequency-dependent selection is known to be caused by differential utilisation of resources[1] or direct interactions between the competitors like nutrient sharing[2] and chemical warfare[3–5]. Here we demonstrate that growth-dispersal trade-offs, in the absence of differences in utilisation of resources and direct interspecies interactions, can also result in frequency-dependent selection due to spatial segregation. The ingredients for spatial segregation are generic and do not require fine-tuned interactions between the populations, therefore enabling frequency-dependent population dynamics for a broad range of populations and environments.

### 4.3 Effects of initial spatial profile

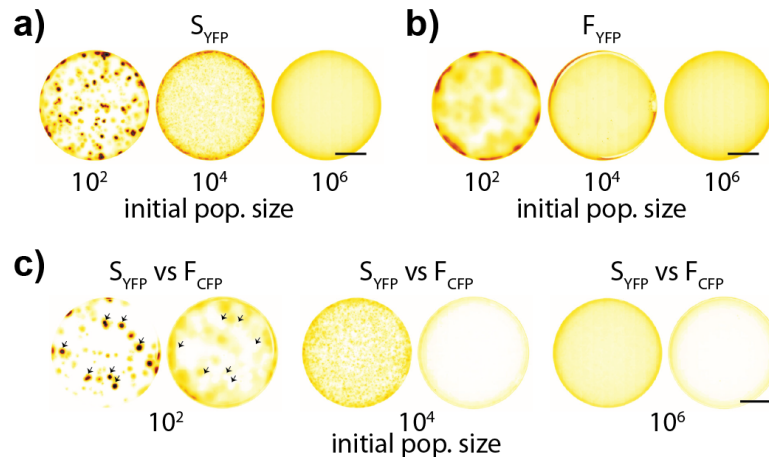


**Figure 4.3: Effects of initial spatial profile.** a) Spatial profiles of population densities after 4 days of  $S_{YFP}$  grown alone. b) Spatial profiles of population densities after 4 days of  $F_{YFP}$  grown alone (the growth and dispersal behaviour of  $F_{YFP}$  is nearly identical to the one of  $F_{CFP}$ ). c) Spatial profiles of population densities of  $S_{YFP}$  vs  $F_{CFP}$ . Black arrows indicate selected peak locations in density of  $S_{YFP}$  and the corresponding valleys in density of  $F_{CFP}$ . Initial population size is given as total number of bacteria. Colour scale: white-yellow-red-black (low to high densities). Scale bar: 10 mm.

So far we focused on point inoculations, i.e. the initial bacterial populations resided within a small region in the centre of the petri dish. Now we lift this restriction and inoculate the initial populations through out the entire petri dish by suspending bacteria within the soft agar gels.

$S_{YFP}$  and  $F_{YFP}$  individually ( $F_{YFP} \approx F_{CFP}$ , as they have comparable growth and dispersal phenotypes) depict similar final density profiles after 4 days of growth (figure 4.3a-b). For large initial population sizes both populations show rather flat density profiles with exaltations close to the edge of the petri dish. For lower initial population sizes the final density profiles become more and more patchy. Remarkably the appearance and structure of patches varies between the two populations. While  $S_{YFP}$  starts forming patches already at intermediate initial populations sizes, patchiness only appears for low initial population sizes for  $F_{YFP}$ . In addition the patches of  $F_{YFP}$  are less rugged than the ones of  $S_{YFP}$ . The observed differences in final population profiles can be rationalised by the absence ( $S_{YFP}$ ) and presence ( $F_{YFP}$ ) of sensing abilities in the two populations. Since  $F_{YFP}$  is able to sense its locally deteriorating environment, it can more efficiently spread out by chasing gradients in nutrients.

Next we test how the final density profiles are altered when the two populations are grown together after being inoculated through out the entire petri dish (figure 4.3c). Again we observe patches to form for small initial population sizes.  $S_{YFP}$  and

$F_{CFP}$  yield specific patterns of ruggedness corresponding to the ones observed when the two populations were grown individually. Interestingly it appears that the two populations mutually exclude each other spatially. Most clear evidence for spatial exclusion can be found for small initial population sizes. Here the pronounced peaks in density of  $S_{YFP}$  distinctly colocalise with valleys in density of  $F_{CFP}$  (see black arrows in figure 4.3c). Avoidance of  $S_{YFP}$  by  $F_{CFP}$  can be readily rationalised by noting that  $S_{YFP}$  acts as a nutrient sink. Local gradients in the nutrient profile are decreasing towards high accumulation of  $S_{YFP}$  and can thus be sensed and avoided by  $F_{CFP}$ . Rationalising the avoidance of  $F_{CFP}$  by  $S_{YFP}$  is less straight forward since  $S_{YFP}$  cannot sense its local environment. The efficient travelling wave colony expansion mode of  $S_{YFP}$  is an emergent phenomenon resulting from an interplay of active random movement and growth. Thus local depletion of nutrient by  $F_{CFP}$  negatively influences growth of  $S_{YFP}$ , hindering it to penetrate into territories occupied by  $F_{CFP}$ . Spatial exclusion, as observed here, has distinct differences to spatial segregation observed for point inoculation. While in the latter case the initial populations are well-mixed and temporal dynamics lead to spontaneous spatial segregation, in the former case the occurrence of patches is already imprinting into the initial spatial profile. In their consequences both are very similar as they result in exclusive access to nutrients within specific areas. Thus spatial exclusion can be viewed as a different type of spatial segregation.

## 4.4 Discussion

Selection pressures acting on motile organisms in spatially structured environments can be altered by an interplay of dispersal and growth. Here we were able to reveal spatial segregation as a key factor shaping selection in space. The occurrence of spatial segregation is general and robust against variations in initial conditions. Initial population size is found to not have a significant effect on the population dynamics, while changes in initial population ratio unveiled a strong frequency dependence of the final competition outcome. Even under substantial changes in the initial population profile, going from point inoculation to spread-out inoculation, the occurrence of spatial segregation remained robust. In summary, the occurrence of spatial segregation is largely independent of the investigated initial conditions and can thus be expected emerge whenever motile populations harvesting growth-dispersal trade-offs compete for resources by invading a non-stirred environment.

Darwin assumed interspecies competition to be key for species development by niche segregation[6]. Here, we have identified a set of sufficient requirements for spatial niche segregation. A sufficiently strong growth-dispersal trade-off and nutrient consumption, in the absence of elaborate interspecies communication or interactions, are sufficient for species to spatially segregate. Our findings may allow to more deeply understand the dynamics of speciation events during the early evolutionary history of life.

Furthermore our results reveal immediate consequence on gut microbial richness, a major determinant of human well-being[7]. The degree to which the spatial structure of the human gut is influencing the composition and richness of its microbiota is still poorly understood, but certainly can have important ramifications for initial gut colonisation and during recovery after antibiotic treatments. In addition understanding microbial exploration strategies holds the promise to create novel anti-pathogen therapies not solely relying on perturbing growth, like traditional antibiotic treatments do, but in addition targeting motility. Specific inhibition of sensory responses or physical jamming of flagella mechanics are potential tools to hinder efficient spreading of pathogens to combat diseases.

### 4.5 Methods

Experimental procedures and bacterial strains are identical to the ones described in chapter 3 aside from one minor difference. While the population sizes shown in chapter 3 are normalised separately within each competition, the population sizes shown in figure 4.1c and 4.2c are normalised to the maximum population size reached by  $S_{CFP}$  when inoculated alone and can thus be compared quantitatively.

## References

- [1] B. R. Levin, *Coexistence of two asexual strains on a single resource*, *Science* **175**, 1272 (1972).
- [2] J. Gore, H. Youk, and A. Van Oudenaarden, *Snowdrift game dynamics and facultative cheating in yeast*, *Nature* **459**, 253 (2009).
- [3] R. Durrett and S. Levin, *Spatial aspects of interspecific competition*, *Theoretical population biology* **53**, 30 (1998).
- [4] B. Kerr, M. A. Riley, M. W. Feldman, and B. J. Bohannan, *Local dispersal promotes biodiversity in a real-life game of rock–paper–scissors*, *Nature* **418**, 171 (2002).
- [5] T. L. Czárán, R. F. Hoekstra, and L. Pagie, *Chemical warfare between microbes promotes biodiversity*, *Proceedings of the National Academy of Sciences* **99**, 786 (2002).
- [6] C. R. Darwin, *On the Origin of Species by Means of Natural Selection, or the Preservation of Favoured Races in the Struggle for Life*, London: John Murray, 1859.
- [7] A. Cotillard et al., *Dietary intervention impact on gut microbial gene richness*, *Nature* **500**, 585 (2013).

## REFERENCES

---



---

## Microfabricated polyacrylamide devices for the controlled culture of growing cells and developing organisms

The ability to spatially confine living cells or small organisms while dynamically controlling their aqueous environment is important for a host of microscopy applications. Here, we show how polyacrylamide layers can be patterned to construct simple microfluidic devices for this purpose. We find that polyacrylamide gels can be molded like PDMS into micron-scale structures that can enclose organisms, while being permeable to liquids, and transparent to allow for microscopic observation. We present a range of chemostat-like devices to observe bacterial and yeast growth, and *C. elegans* nematode development. The devices can integrate PDMS layers and allow for temporal control of nutrient conditions and the presence of drugs on a minute timescale. We show how spatial confinement of motile *C. elegans* enables for time-lapse microscopy in a parallel fashion.

### 5.1 Introduction

The ability to create precisely controlled microenvironments has been pursued in microbiology[1], cell biology[2] and tissue engineering[3]. Microfluidic techniques have emerged as an important tool to impose spatial confinement, while allowing controlled delivery of nutrients and drugs, and drastically increase the level of

---

The content of this chapter has been previously published as "Philippe Nghe, Sarah Boulineau, Sebastian Gude, Pierre Recouvreur, Jeroen S. van Zon, and Sander J. Tans - Microfabricated Polyacrylamide Devices for the Controlled Culture of Growing Cells and Developing Organisms, PLoS ONE 8(9): e75537, 2013"

parallel data acquisition[4, 5]. Controlled delivery is important for observing cellular responses to external changes, but also to continuously replenish consumed compounds and depleting secreted waste that may become toxic. Realizing these features often requires complex device designs to separate the fluid flow from the observation chambers, involving multiple micro-structured layers, surface treatments and multiple modules[1–3, 5], which can limit their applicability[6].

PDMS-based microfluidic devices are extremely versatile and have been applied to the culture of bacteria[7], yeast[8], mammalian cells[9], and even embryos[10] or nematode worms[11]. While allowing for exquisite control of flows, PDMS based devices often require sophisticated designs to achieve both confinement and controlled culture conditions and can ultimately be limited by the properties of PDMS as a material. PDMS devices can ensure localization of the object under study by confinement in micro-chambers and controlled medium exchange by laterally connecting channels that are narrow enough to prevent escape of the cells[12, 13]. However, this typically requires multi-layered flow-cell designs and sometimes integration of in situ valves[14]. Watertight closure of the system is generally performed by plasma treatment of the PDMS[15], which can be incompatible with complementary treatments required to obtain the stable hydrophilic or hydrophobic properties ensuring appropriate adhesion of cells to the surfaces of the culture chambers[16]. PDMS is not permeable to aqueous solutions[15], which is desirable in some applications but a limitation in others, as it does not allow building osmosis or dialysis membranes, and can lead to local medium heterogeneities[17, 18] and accumulation of toxic residues[19]. In addition, PDMS has poorly tunable mechanical properties, which are critical for the correct growth of many cell types[20, 21].

Many of these issues could be addressed by the use of hydrogels. Hydrogels allow for free diffusion of the medium throughout the device, thereby ensuring uniformity of the cellular environment. In addition, hydrogels have highly tunable mechanical properties[22]. For these reasons, a variety of micro-environments based on hydrogels are being explored for tissue engineering[3, 23]. So far, the most commonly used hydrogel for the study of micro-organisms as well as multicellular organisms is agarose, which is commonly used as an "agar pad", a single monolayer of hydrogel, to support the growth of bacteria[24], yeast[25] or nematodes[26, 27] in the imaging plane for live microscopy imaging. Simple layers of agarose have also recently been used as membranes to control bacterial medium in time[28–30]. In addition, agarose has been structured on the micrometer scale, e.g. to create grooves that guide the growth of bacteria[31, 32] or to build microchambers to spatially confine live nematode larvae[33]. However, agarose is brittle and tears readily, making it difficult to manipulate, especially in the form of thin layers, which ultimately limits microfabrication possibilities ([34], personal communication with the authors). In addition, agarose is composed of sugars and can be directly metabolized by some organisms[35] or may contain residual non-purified simple sugars, which could interfere with the study of growth under well-controlled conditions.

Here we propose polyacrylamide hydrogels as an alternative substrate for build-

ing controlled micro-environments. Polyacrylamide gels have several practical advantages that make them ideally suited for developing devices for live microscopy in biological studies. First, polyacrylamide is a commonly used material in biology laboratories for DNA and protein electrophoresis and its microfabrication requires minimal technological investments, as we will show below. Polyacrylamide gels are physico-chemically well-characterized and known to be biocompatible[36, 37]. They are mechanically stronger (typical fracture energy  $G \approx 10\text{-}50 \text{ J.m}^{-2}$ [38]) than agarose gels ( $G \approx 0.1\text{-}6 \text{ J.m}^{-2}$ [39, 40]) and hence allow for easier handling and are better suited for microfabrication. Their elastic properties are tunable over a wide range (from a fraction to several tens of kPa) by changing the total acrylamide content and the acrylamide to bis-acrylamide ratio[37], which allows for the construction of cell culture matrices with well-controlled mechanical properties[36, 41, 42]. They are permeable to aqueous solutions and composed of a synthetic polymer that cannot be metabolized as a carbon source, which allows for excellent control of the growth conditions. While polyacrylamide gels have been photopolymerized inside glass microchannels for in situ microfabrication[43], to build miniaturized electrophoresis devices[44, 45] or inside PDMS channels to create flat cell culture matrices with elasticity gradients[46], their unique properties have not yet been exploited to construct micro-structured devices for biology studies using standard soft lithography techniques.

Here, we demonstrate two essential properties of polyacrylamide gels that enable the building of controlled environments and can be used simultaneously. First, we describe a soft lithography method to transfer micropatterns, such as confining culture chambers and microchannels, from a silicon wafer to a polyacrylamide gel. Second, we show how to use polyacrylamide gels as membranes to control the transfer of chemicals, building on previous designs using other materials that use dialysis membranes to change medium in time[47] or that use diffusion between lateral channels to generate gradients in space[34, 48]. We describe several elementary designs, which consist of a polyacrylamide membrane constrained between glass or PDMS components, and demonstrate their use for the study of a range of organisms. We show that one can control the growth of *E. coli* bacterial colonies by controlling the carbon source as a function of time, and simultaneously track the response on the level of single-cell lineages. We also show that we can confine and grow *S. pombe* yeast cells, imposing a time-controlled reversible depolymerization of microtubules by a drug. Finally, we show that we can confine *C. elegans* nematode larvae in microchambers and follow the growth of multiple individual larvae in parallel by time-lapse microscopy.

## 5.2 Microfabrication of polyacrylamide gels

**Master mold.** Microfabricated polyacrylamide membranes can be indefinitely reproduced by soft-lithography from a single silicon wafer comprising the desired

micropattern made of an epoxy resin, such as SU-8 (Methods). The initial master mold was made according to standard protocol by UV-lithography from a printed transparent mask, allowing the specification of an arbitrary two-dimensional pattern with a uniform height determined by the user, typically ranging from 1 to 100 microns.

**Molding of the acrylamide.** The aqueous solution of acrylamide monomers mixed with curing agents is poured on the master mold within a contour made of glass or metal of predetermined height, bound to the wafer with silicon grease (Methods, Figure 5.6). The molding cavity is then closed with a silanized glass coverslip. A gel is generally obtained after 20 min at room temperature, but waiting 2 h ensures optimal polymerization. After polymerization, this results in a polyacrylamide gel with one face shaped as the negative of the micropattern of the master mold. We could easily obtain replica of molds going down to 10 micron features with an apparent fidelity at the micron scale (Figure 5.7). Note that we also use unstructured flat polyacrylamide membranes in the following. These are obtained according to the same protocol in which the wafer has been replaced by a silanized glass slide.

**Preparation of the polyacrylamide membrane.** After polymerization, the top silanized coverslip is removed, after which the gel is cut to the experimentally required dimensions and removed with tweezers. Importantly, the polyacrylamide membranes should be rinsed in water to remove unpolymerized acrylamide monomers, which are in particular known for their neurotoxicity. Proper rinsing has already been demonstrated to ensure biocompatibility of polyacrylamide matrices for neuron growth and development for weeks[49]. Transferring the polyacrylamide layer to fresh purified water at least two times for approximately 1 h proved sufficient to ensure the absence of observed growth defect in the organisms studied in this article. The membrane can be stored for several weeks in an aqueous solution without detectable degradation, consistent with quantitative studies of long term polyacrylamide degradation[50]. Before using the polyacrylamide membrane for a cell or organism culture experiment, we soaked it two times in the appropriate medium.

### 5.3 Experimental designs

In Figure 5.1, we first outline the different designs used in this research. In general, all devices consist of multiple layers stacked on top of each other, with the entire device being held together by mechanical clamping (Figure 5.1). In our case, this clamping was achieved by a metal holder with screws, with the appropriate openings for microscopy acquisition and microfluidic connectors.

In all different designs the objects under study are confined between the polyacrylamide membrane and the glass coverslip through which microscopy imaging is performed. Here, we use two different approaches to achieve this. In the first design, we enclose the membrane within a surrounding glass spacer sealed to a

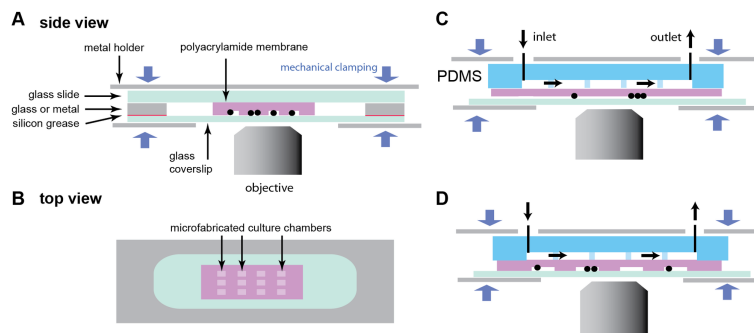


**Figure 5.1: Schematics of devices for cells or organisms culture in polyacrylamide membranes.** In all devices presented here, the different layers are held together by mechanical clamping, and the cells or organisms (represented as black circles) grow at the interface between the polyacrylamide gel and a glass coverslip through which microscopy is performed. (A) Side view of a microfabricated membrane comprising culture chambers, mechanically clamped between a glass slide and a glass coverslip. The device is sealed with a glass or metal contour. Sealing can be enhanced by adding vacuum silicon grease between surfaces. (B) Top view of panel A showing the array of microchambers surrounded by the glass or metal contour. (C) Flow cell using a PDMS control channel in contact with a polyacrylamide monolayer, which allows transfer of the flowing medium to the cells. In this design, cells are compressed underneath a flat polyacrylamide monolayer. (D) A more complex device combining the microchambers of the design in panel A and with the PDMS control channel in panel C.

top glass slide with vacuum silicon grease (Figure 5.1A, B). This simple design ensures sufficient airtightness to limit evaporation and allows for observation under constant conditions for at least two days, provided that nutrients in the hydrogel membrane are present in excess. In the second design, a PDMS device containing a control channel is placed on top of and in direct contact with the polyacrylamide membrane (Figure 5.1C), thereby allowing continuous diffusion of the medium to cells or organisms growing below the hydrogel membrane. With this type of design, flow rates of a few tens of  $\mu\text{L min}^{-1}$  allow one to switch the media within seconds, generating pressures below 100 Pa, allowing continuous use without leakage for at least a day. As the mechanical clamping used in all these designs avoids irreversible sealing or chemical bonding, the PDMS channel can be re-used many times.

Potentially, microfabricated polyacrylamide membranes and PDMS control channels can be combined depending on the experimental needs (Figure 5.1D). Possible designs are not limited to those in Figure 5.1: as an example we demonstrate below a device with channels embedded in the membrane.

## 5.4 Temporal and spatial control of the microenvironment

First, we used the advantageous transport properties of polyacrylamide gels to precisely control the medium composition in time, using an unstructured gel as a membrane, as well as in space, by setting up a concentration gradient within a membrane comprising molded microchannels.

In the first experiment, time control of the medium was obtained by placing a 500  $\mu\text{m}$  thick gel membrane between a structured PDMS layer and a glass coverslip (Figure 5.2A). Flow was established in the PDMS channel with a syringe pump at flow rates ranging between 20 and 50  $\mu\text{L min}^{-1}$ . A fluorescent glucose analog (2-NBDG) was added or removed from the flowing medium at a particular time point by switching a valve, thereby changing the composition of the flowing medium within seconds. The amount of 2-NBDG fluorescence was measured as a function of time by standard fluorescence microscopy using a 100X objective focused on the gel-glass interface. After the change of medium, the measured fluorescence signal rose in an approximately exponential fashion to the newly imposed steady-state value with a half-time of  $\approx 5$  min (Figure 5.2B, C). Fits to the diffusion profile (Methods) yielded diffusion coefficients of  $4.0 \times 10^{-10} \text{ m}^2 \text{ sec}^{-1}$  to  $5.3 \times 10^{-10} \text{ m}^2 \text{ sec}^{-1}$ , comparable to the typical diffusion coefficient of small molecules in water ( $\approx 5.0 \times 10^{-10} \text{ m}^2 \text{ sec}^{-1}$ ).

In the second experiment, we aimed to set up a spatial concentration gradient by placing a structured gel membrane between a glass slide and a flat PDMS layer, the latter containing inlet and outlet connectors (Figure 5.2D). Liquid was pumped through the 100  $\mu\text{m}$  high channels molded into the polyacrylamide hydrogel at 50  $\mu\text{L min}^{-1}$ . One channel contained pure water, whereas the other contained an aqueous solution of fluorescein molecules. Diffusion of fluorescein into the polyacrylamide hydrogel, coupled with its removal at the adjacent channel, gave rise to a linear concentration gradient in the space between the two channels[34]. We found that the spatial gradient reached steady state after  $\approx 1$  h. Subsequently, we imaged the concentration profile at mid-channel-depth. We observed a linear concentration gradient within the gel between the two channels as predicted by the theory (Figure 5.2E, F)[34].

## 5.5 Carbon controlled growth of bacteria

We tested the use of the polyacrylamide hydrogels to create a microfluidic chemostat for the growth of *E. coli* bacteria (Figure 5.1C). First, we used time-lapse phase contrast microscopy to visualize single *E. coli* cells growing on a simple flat polyacrylamide membrane while flowing minimal medium with abundant lactose. Cells divided for at least 8-9 generations into mono-layered colonies (Figure 5.3A). Given the absence of overlap between cells in the imaging plane, we could perform unambiguous determination of their outlines and determine the length of individual

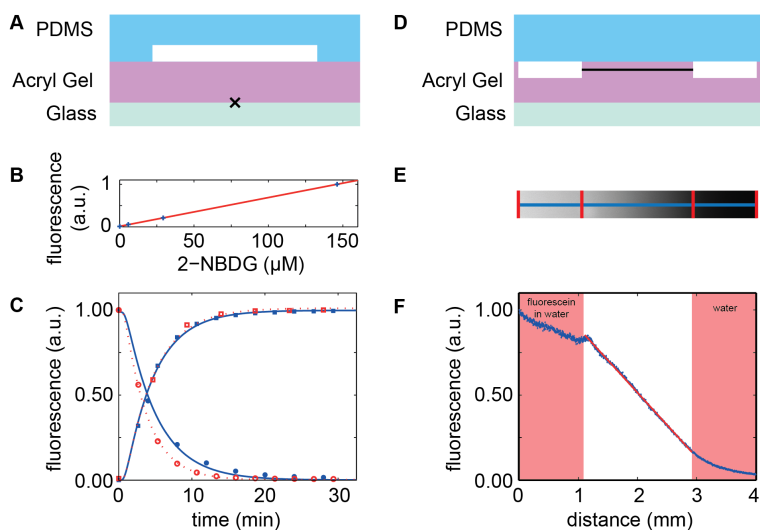


**Figure 5.2: Diffusion in unstructured and structured polyacrylamide hydrogel membranes.** (A) Sketch of the flow cell device. An unstructured acryl gel (height  $500\ \mu\text{m}$ ) is sandwiched between a PDMS layer comprising a channel (height  $113\ \mu\text{m}$ ), and a glass coverslip, similar to the design in Figure 5.1A. (B) Fluorescence of the small dye 2-NBDG is proportional to its concentration in the flowing solution. (C) Fluorescence signal after infusion (squares) or depletion (circles) of the dye 2-NBDG was measured at the gel-glass interface (black cross in A). Lines show fits to the 1D diffusion equation. Open symbols and dashed lines correspond to flow rates of  $50\ \mu\text{L}\ \text{min}^{-1}$ , closed symbols and solid lines to flow rates of  $20\ \mu\text{L}\ \text{min}^{-1}$ . (D) Sketch of the linear gradient generator device. A structured polyacrylamide hydrogel (height  $1\ \text{mm}$ ) is sandwiched between a PDMS layer and a glass slide. Water containing  $3.5\ \mu\text{g}\ \text{ml}^{-1}$  fluorescein is flown through the left channel, while pure water is flown through the right channel, thereby creating a linear concentration gradient within the gel. (E) Image of the fluorescence intensity profile at mid-channel height (black line in D) taken 85 min after the flows were established. Red lines indicate channel walls. (F) Fluorescence intensity profile (blue crosses) plotted versus distance (along the blue line in E). The fluorescence intensity in the acryl gel in between the channels is linear (red line).

cells using custom image analysis software (Figure 5.3B, Methods). The population growth, quantified as the sum of the length of all cells in the microcolony, showed that cells were growing exponentially (Figure 5.3C, green trace) with a doubling rate of  $\approx 0.9\ \text{h}^{-1}$ .

Control of the growth rate of bacterial cells was demonstrated by exponential growth on minimal medium supplemented with various carbon sources (Figure 5.3C). The population growth showed that cells grew at a constant rate in each condition, yielding doubling rates of  $0.8\ \text{h}^{-1}$  for growth on maltose (Figure 5.3C, red trace),  $0.6\ \text{h}^{-1}$  on lactate (Figure 5.3C, yellow trace) and  $0.23\ \text{h}^{-1}$  on limiting lactose (Figure 5.3C, blue trace). These values are in good agreement with our growth rate measurements in bulk (Figure 5.8) and the relative quality of the different carbon

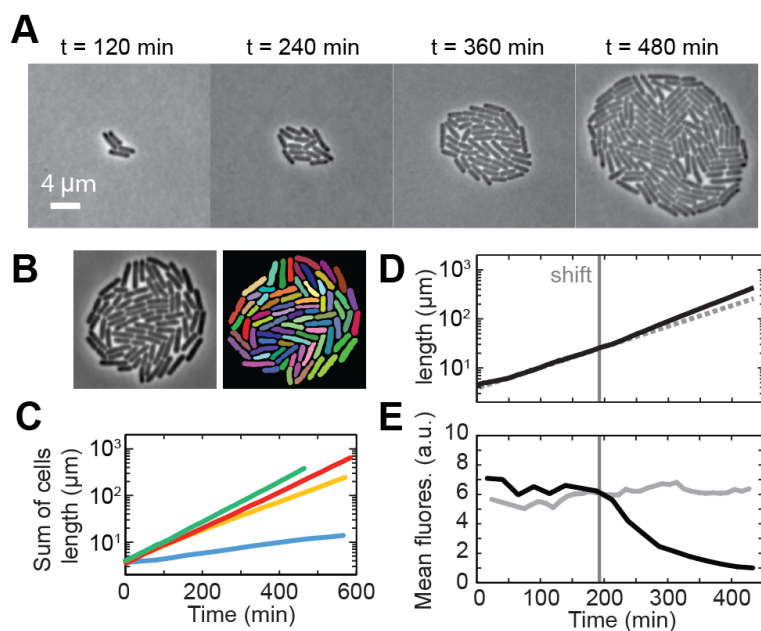


**Figure 5.3: Monitoring bacterial growth by time-lapse microscopy.** (A) Phase contrast images of *E. coli* cells growing in minimal medium supplemented with lactose. (B) Typical cell detection performed on a phase contrast image. (C) Sum of cells length for microcolonies growing on minimal medium with lactose (green), maltose (red), lactate (yellow) and limiting lactose (blue) as sole carbon source. (D) Sum of cells length during a shift from lactose to glucose and (E) corresponding mean fluorescence intensity of the colony. For comparison, fluorescence intensity for a colony growing only on lactose is shown in grey.

sources ([51] and Methods). Growth on limiting lactose confirmed in particular that the nutrient-free polyacrylamide matrix is suitable for attaining and studying low growth rates.

To show the ability of our designs to study cell dynamics in changing environments, we performed a carbon shift (with the device of Figure 5.1C as described in Section 3), and monitored both growth and gene expression over time. We started from a single cell on a minimal medium containing lactose, and switched to a minimal medium containing glucose after three generations. Expression of the *lac* genes was measured with a GFP reporter inserted in the *lac* operon (see Methods). The *lac* genes control the import and catabolism of lactose and are induced during growth on lactose, but repressed when glucose is present.

We show the population-level dynamics in Figure 5.3D-E. During growth on lactose, cells reached a steady state growth rate of  $0.8 \text{ h}^{-1}$  and the mean fluorescence intensity of the microcolony per unit area over time was high, consistent with the full expression of the *lac* genes in all cells. Upon shifting to glucose, the growth rate was maintained at its pre-shift value during approximately 20 min, after which it increased abruptly to the higher glucose steady-state value of  $1 \text{ h}^{-1}$ . At the same time, the mean fluorescence started to decrease exponentially with a characteristic



half time of 70 min, close to the doubling time. This indicated that upon the arrest of lac genes expression after the shift, the decrease in GFP intensity per unit area signal was dominated by dilution[51], until attaining cellular auto-fluorescence levels after four generations. Overall, these experiments indicate that polyacrylamide gels allow for controlled and prolonged growth for constant nutrient conditions, and in response to a change in nutrient conditions.

## 5.6 Temporary depolymerization of microtubules in yeast by a drug

To explore the application of polyacrylamide devices to observe fission yeast, we first investigated whether they grew normally, both between an unstructured hydrogel monolayer and a glass cover slip and confined within microstructures such as channels or chambers in a device similar to Figure 5.1A-B. When cells were positioned between an unstructured flat hydrogel and a glass coverslip, we could observe constant exponential growth of the fission yeast cells for more than 7 generations over 20 h (Figure 5.4A). This corresponded to an average doubling time of 170 min at  $32\pm 1/2^{\circ}\text{C}$ , in agreement with liquid culture growth rate in the same minimal medium. This indicated that the mechanical pressure imposed by the hydrogel layer was soft enough to not perturb growth.

We then grew yeast cells, which have a 3-4  $\mu\text{m}$  diameter, confined in 3  $\mu\text{m}$  deep microstructures molded in the hydrogel. Time-lapse imaging showed that colony expansion was constrained by the walls (Figure 5.4B).

We tested the ability of the microstructured membrane to control the chemical composition of the microenvironment, using a PDMS control channel on top (Figure 5.1D). Here we aimed to induce microtubule depolymerization with the drug methyl-2-benzimidazole-carbamate (MBC) during a certain time window. In fission yeast cells, microtubules form 3-5 bundles composed of groups of 2-4 microtubules. After growing yeast cells for 2 generations, we supplemented the flowing medium with 50  $\mu\text{M}$  of the microtubule-destabilizing drug. Within 5 min, the fluorescently (GFP) labelled microtubules had disappeared in more than 80% of the cells (Figure 5.4C). In the remaining fraction of cells, abnormally short microtubules were present, as already reported for MBC-treated fission yeast cells[52]. After 60 min, the drug was removed from the flowing medium, leading to the reappearance of microtubules in more than 90% of cells within 5 min.

In conclusion, we have shown that yeast cells grow normally on polyacrylamide hydrogel membranes, and that colony expansion can be confined between a flat hydrogel membrane and a glass coverslip, or within a structured membrane. The membrane allowed for adding or removing a drug on a timescale of minutes.

## 5 Microfabricated polyacrylamide devices for the controlled culture of growing cells and developing organisms

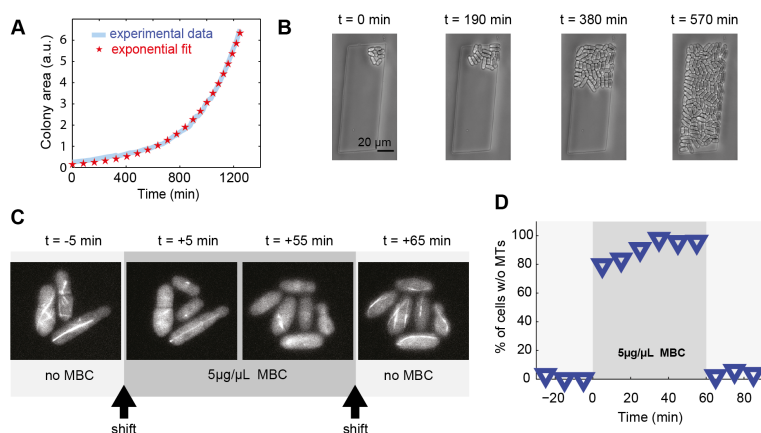


**Figure 5.4: Control of the microenvironment of growing fission yeast colonies.** (A) Growth curve of the colony (area) obtained by a time-lapse experiment (blue) from 1 cell to 142 cells after 20 h. In red, single exponential fit of the growth rate with a doubling time of 240 min. (B) Phase contrast images of the fission yeast *S. pombe* growing in a microchamber. (C) Fluorescent microscopy images of fluorescently labeled microtubules during treatment with the microtubule-inhibiting drug methyl-2- benzimidazole-carbamate (MBC). Before the injection of 5 µM MBC, microtubules are observable in every cells ( $t = -5$ min). 5 min after the shift microtubules disappeared in more than 80% of the cells. MBC treatment lasts for 1 h, over which microtubule assembly is not observed. Rapidly after the wash out of the drug, microtubules reappeared in almost every fission yeast cell. (D) Percentage of cells without observable microtubules in a time-lapse experiment, before, during and after microtubule depolymerization with 5 µM of MBC.

### 5.7 Growth and development of spatially confined *C. elegans* larvae

Next, we aimed to investigate whether our devices can be used to monitor the growth and development of single larvae of the nematode worm *Caenorhabditis elegans*. Hence we enclosed *C. elegans* worms in an array of microchambers molded into polyacrylamide hydrogel (Figure 5.5A).

We positioned one *C. elegans* egg per microchamber together with *E. coli* bacteria as food source, and followed multiple chambers by time-lapse microscopy. The eggs were found to develop inside the polyacrylamide microchambers and newly hatched larvae increased in length from about 150 µm directly after hatching to about 350 µm over the course of 10-15 h (Figure 5.5A and B). Despite their active motility, all larvae stayed confined to the microchambers during the entire period of observation.

Development of *C. elegans* is divided in four larval stages, labeled L1 to L4, that are separated by molts during which a new cuticle is synthesized and old cuticle is shed. The molts are accompanied by a behaviorally quiescent state called lethargus. After 10-15 h, animals entered the lethargus accompanying the L1 molt (Figure 5.5B), agreeing well with the observed duration of the L1 larval stage of 15 h[26]. We

observed that the start of the L1 molt correlated well with animal length: the observed variability in the time of entry into the L2 lethargus was mostly due to variation in animal length at the time of hatching. These results indicate that the nematodes were able to develop to the L2 larval stage inside the microchambers.

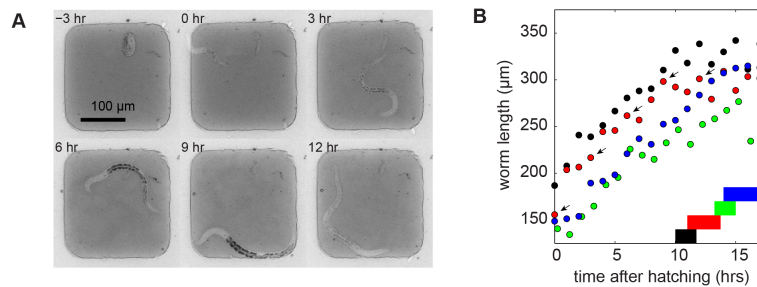


**Figure 5.5: *C. elegans* growth in microchambers.** (A) Growth of a single *C. elegans* animal through the L1 larval stage constrained in a 200 x 200 x 18  $\mu\text{m}$  polyacrylamide microchamber filled with OP50 as source of food. Time is shown in hours after hatching. At 12 h after hatching the animal has entered the lethargus at the end of the L1 larval stage. (B) Worm length as a function of time after hatching. Different colors indicate animals grown in parallel on the same device. Horizontal bars show the duration of lethargus, ending with the molt at the start of the L2 larval stage. The markers indicated by the arrow correspond to the time points shown in (A).

## 5.8 Discussion

We have demonstrated the microfabrication of structured polyacrylamide membranes by soft-lithography and used these to build controlled environments for the study of growing cells and organisms. While similar capabilities can be achieved with other techniques based on agarose gels or PDMS, our method has several practical advantages. Agarose layers can easily tear, while the mechanical strength of polyacrylamide allows easy handling of the gel during microfabrication steps and assembling the flow cell, and provides high success rates, reproducibility, and well-defined structural features. We found that polyacrylamide membranes down to 140  $\mu\text{m}$  thickness could be used routinely. In contrast, we found that agarose layers of the same thickness and elastic modulus (50 kPa for 1% agarose[39]) systematically broke down during the fabrication process. In comparison to PDMS-based devices, which often involve more complex multi-layer lithography to define feeder channels, our method is simple and requires minimal investment in materials and technological infrastructure. Our protocol for fabrication of polyacrylamide hydrogels is commonly used in biology laboratories for protein electrophoresis and involves preparation of a solution that polymerizes at room temperature. Once polymerized, these membranes remain functional for months when stored in solution. The microfabrication step relies on a silicon mold that can be re-used multiple times.

We have tested various device-designs which allow accurate spatio-temporal control of the environment. Control in time was achieved by diffusion of the medium through the permeable gel into culture chambers that are hence uncoupled from the medium flow. Diffusion coefficients of small molecules in the gel are close to their value in water, which combined with the possibility to build thin membranes resulted in a medium exchange with a characteristic time of 5 min. This response time is well-suited for many applications that require the control of the growth and gene expression dynamics in micro-organisms such as bacteria or yeast. We demonstrated the creation of linear concentration gradients between two continuously flowing solutions in channels embedded in a single gel layer. This method may be used to set up gradients that are steeper or have more complex two-dimensional patterns than flow-cells used so far. In these existing designs, diffusion between PMDS channels is indeed constrained to occur through an unstructured agarose layer in a third dimension[34]. We have demonstrated the potential of these devices to study dynamically the genetic or the morphologic responses to changes in growth medium or the addition of chemical inhibitors of cellular processes. In conclusion, polyacrylamide-based devices are well suited to study the response of diverse biochemical pathways to chemical perturbations. They are well suited for metabolism and growth studies as the polyacrylamide matrix is free of nutrients.

We found that bacteria and yeast grew in well-defined monolayers when covered with polyacrylamide, as is also observed for agar pads, thus allowing convenient microscopy and analysis at the single cell level. The soft confinement provided by the polyacrylamide membranes ensured localization of the colonies, while maintaining normal growth and morphological phenotypes without requiring the deposition of an additional soft layer on the glass[47]. In our case, experiments were stopped when the colonies developed a second layer. For slow-growing cells, the devices allow observation of exponential growth for over 2 days. Longer term experiments, such as used to study aging, would require one to adapt designs including washing channels (see 54,55 for PDMS and[32] for agarose realizations). In addition, polyacrylamide allows chemical modifications for the control of the micro-environment, enabling advanced capabilities such as the controlled release of bacteria[53] or patterned bio-functionalization[54].

The technology is also promising for the study of larger, multicellular organisms, such as *C. elegans*. Polyacrylamide gels with microchambers provide important advantages. First, they allow spatial confinement of these otherwise highly motile organisms, enabling time-lapse microscopy and parallel image acquisition without the use of anesthetic drugs[27] or automated tracking of individual animals[55]. Second, polyacrylamide hydrogels enable exchange of medium and waste products with the microenvironment of the animal.

Finally, the tunable mechanical properties of polyacrylamide hydrogels make them potentially useful for the culture of other cell types, given for example the exquisite sensitivity of mammalian cells to the mechanical properties of their support[20]. The potential to embed microfabricated polyacrylamide membrane in

complex modular designs offers exciting opportunities to develop well-controlled environments for cell biology studies and tissue engineering.

## **5.9 Methods**

### **5.9.1 Fabrication**

Master molds have been realized on silicon wafers with spin-coated SU-8 epoxy resins (MicroChem) of different viscosities (models 2005, 2025 and 2100) resulting in heights of 3  $\mu\text{m}$  for the yeast chambers, 18  $\mu\text{m}$  for the worm chambers and 100  $\mu\text{m}$  for the gradient assay. No specific wetting treatment was done to the surface of the wafer. For the polyacrylamide gel, we used a 29:1 ratio of acrylamide / bis-acrylamide (Bio-Rad) with a final concentration of 10%. Polymerization was initiated by the addition of 0.1% of ammonium persulfate (Sigma) and 0.1% of TEMED (Sigma). The mixture was poured in a mold consisting of a cavity made of a machined glass or aluminum slide of thickness varying between 150  $\mu\text{m}$  and 1 mm, glued to the wafer or to a simple silanized glass slide with vacuum silicon grease. A silanized glass coverslip was deposited on top and the solution was left to polymerize for about 2 h. The polyacrylamide membrane was then cut and transferred in DI water for conservation. The PDMS (Dow Corning) channel was molded on a silicon wafer with SU-8 according to the protocol provided by the resin manufacturer (MicroChem) and consisted of a 113  $\mu\text{m}$  high and 5 mm wide channel comprising pillars to ensure uniformity of the pressure applied on the polyacrylamide membrane. Mechanical clamping of the whole device was ensured by a home-made metal holder with 4 screws, comprising openings on the bottom for microscopy acquisition and on the top for illumination and the tubing. To ensure a good seal between the polyacrylamide and the PDMS layer, we made sure that the hydrogel and the PDMS had a contact area that extended at least 3 mm away from the edges of the control channel.

### **5.9.2 Experimental devices**

The flow was externally driven with syringe pumps (ProSense, NE-1000 and NE-300) connected to the microfluidics device by polyethylene tubing of 0.58 mm internal diameter (Smiths medical International Ltd.). When using a PDMS channel, the device was degassed 1 h in low vacuum prior to flow to allow removal of trapped air bubbles by suction from the PDMS matrix. Switches were performed by a manual valve (Hamilton, HV 4-4). All experiments have been performed with an inverted epifluorescence Nikon microscope TE-2000 U embedded in a temperature controlled box.

### 5.9.3 Bacteria

Growth experiments were performed using derivatives of *E. coli* MG1655 (rph-1 ilvG- rfb-50). To measure the expression of the lac operon, lacA was replaced with GFPmut2 (kindly provided by M. Ackermann, ETH Zürich). Cells were grown in M9 minimal medium (47.7 mM Na<sub>2</sub>HPO<sub>4</sub>, 25 mM KH<sub>2</sub>PO<sub>4</sub>, 9.3 mM NaCl, 17.1 mM NH<sub>4</sub>, 2.0 mM MgSO<sub>4</sub>, 0.1 mM CaCl<sub>2</sub>) with 0.2 mM uracil, supplemented with 0.1% (w/v) lactose, maltose or lactate and 0.001% (w/v) lactose in the limiting case. Note that adding uracil compensates for intrinsic pyrimidine starvation of the MG1655 strain[56] and accounts for the typically 15% higher growth rates measured in our study compared to Beg & al[51]. Cells were initially inoculated from glycerol stock in TY medium and grown until the OD > 0.02 and next diluted in the appropriate medium overnight. The following day, the overnight culture was diluted in the same medium (OD 0.005) and transferred to the microfluidic chamber. 10  $\mu$ L of culture were deposited on the polyacrylamide gel membrane and left to dry for about 2 min before the setup was assembled. Optionally, addition of a surfactant in the medium (Tween 20 at 10<sup>-5</sup> volume fraction) allowed further enhancement of colony growth into a monolayer. All these steps and the experiment were performed at 37°C. Images were acquired with a 100X oil immersion objective (Nikon, Plan Fluor NA 1.3). Phase contrast and fluorescence images were analyzed with a custom Matlab algorithm derived from an algorithm of the Elowitz lab (Caltech)[57]. The instantaneous growth rate was determined by fitting the cell length over time to an exponential function.

### 5.9.4 Yeast

For growth experiments, we used the *S. pombe* wild type fission yeast PT286 h-ade6-M216 leu1-32 ura4-D18. For the pad growth experiment, fission yeast cells were pre-grown overnight in Edinburgh Minimal Medium (EMM) liquid culture. 2  $\mu$ L of 10x-concentrated culture were deposited on a polyacrylamide gel membrane that had been incubated in EMM medium. All these steps and the experiment were performed at 32°C. Cells were imaged through a 40X objective oil immersion lens (Nikon, NA=1). Colony area was measured with ImageJ (<http://rsbweb.nih.gov/ij>) software. For the drug shift experiment, the same culture conditions were used for a strain expressing GFP tubulin (DB 871 h90 nmt1-GFP-tub:lys1+ leu- ura-) and microtubule detection was performed visually. For the confined growth experiment, we used a YE5S medium and performed imaging with a 20X objective (Nikon, NA=0.5) at 37°C.

### 5.9.5 Nematodes

The wild-type (N2) *C. elegans* strain was grown on NGM agar plates covered with *E. coli* OP 50 as food source, following standard protocols[58]. Before sample

preparation, the polyacrylamide microchamber array was soaked overnight in M9. Under a stereomicroscope, OP 50 bacteria and a single embryo at the three-fold stage, between 550 and 840 min after fertilization[26], were transferred to each individual microchamber, using a worm pick to transfer bacteria and an eyelash attached to a Pasteur pipet to transfer eggs. Images of individual microchambers were captured every 15 min using a 10X Nikon objective (NA=0.30). L1 larvae hatched and developed at room temperature (22±½C). Worm length was quantified as a function of time with a 1 h interval. Entry into and exit from the L1 molt was monitored by eye, based on the reduction in movement during lethargus, the decrease in contrast in the transparency of the animal's body due to synthesis of the new cuticle and finally the shedding of the old cuticle.

### 5.9.6 Fitting of diffusion coefficients in Figure 5.2C

Formula was taken from Crank[59]:

$$C = C_0 \left( \sum_{n=0}^N (-1)^n \operatorname{erfc} \left( \frac{(2n-1)l-x}{2\sqrt{Dt}} \right) + \sum_{n=0}^N (-1)^n \operatorname{erfc} \left( \frac{(2n-1)l+x}{2\sqrt{Dt}} \right) \right) \quad (5.1)$$

where  $l = 500 \mu\text{m}$  (width of system),  $x = 0 \mu\text{m}$  (position of measurement),  $C$  is concentration and  $t$  is time, values taken from Figure 5.2C. Fitting was performed with Matlab with  $N = 3$ . The maximum concentration  $C_0$  and the diffusion coefficient  $D$  were used as fitting parameters.

## 5 Microfabricated polyacrylamide devices for the controlled culture of growing cells and developing organisms

---

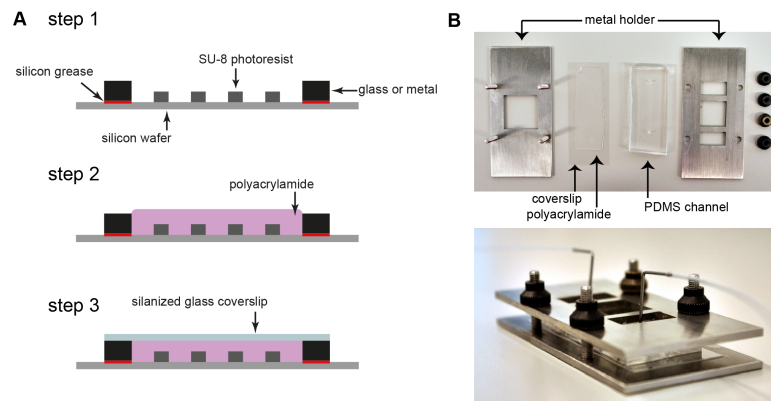


**Figure 5.6: Molding of the polyacrylamide gel and assembly of the device.** (A) Step 1: A cavity is prepared, consisting in the silicon wafer with the photoresist pattern, reversibly assembled with vacuum grease to a glass or metal contour of desired height. Step 2: The acrylamide solution is injected with a pipette within the cavity. Step 3: A silanized coverslip is then added on top of the cavity and polymerization occurs at room temperature for 2 h. (B) Photographs of a multi-layered device: separate parts (top) and assembled device (bottom).



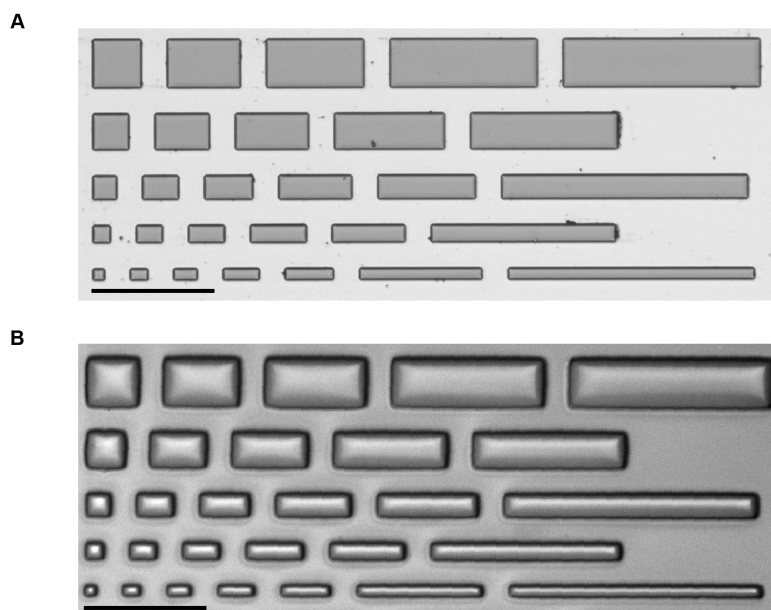


**Figure 5.7: SU-8 pattern on a wafer and molded acrylamide gel.** (A) Image of a silicon wafer with 3  $\mu\text{m}$  high patterns in SU-8 photoresist. (B) Structures shown in A have been molded in a polyacrylamide gel. Scale bars 100  $\mu\text{m}$ . The smallest features are 10  $\mu\text{m}$  wide.

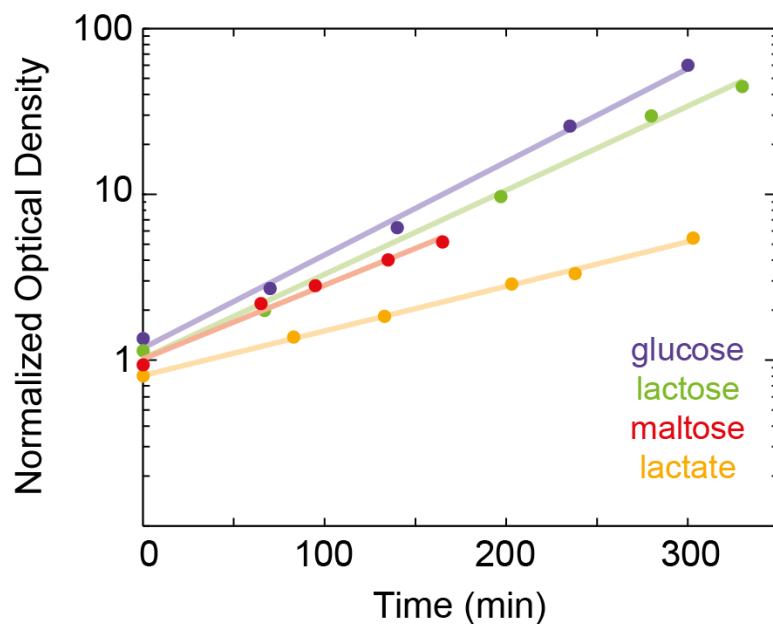


**Figure 5.8: Growth rates in batch cultures.** Optical density at 550 nm normalized by the OD at  $t=0$  (and shifted for clarity) versus time for batch cultures of MG1655 cells growing in minimal medium with abundant (0.1%) glucose (blue), lactose (green), maltose (red) and lactate (yellow) as sole carbon source. Exponential fits to the experimental data points (lines) yielded growth rates of  $1.12 \text{ h}^{-1}$  on glucose,  $1.01 \text{ h}^{-1}$  on lactose,  $0.88 \text{ h}^{-1}$  on maltose and  $0.54 \text{ h}^{-1}$  on lactate, comparable to those obtained for cells growing in the microfluidic device (see main text and Figure 5.3B and D).

## References

- [1] D. Weibel, W. Diluzio, and G. Whitesides, *Microfabrication meets microbiology*, *Nat Rev Microbiol* **5**, 209 (2007).
- [2] J. El-Ali, P. Sorger, and K. Jensen, *Cells on chips*, *Nature* **442**, 403 (2006).
- [3] A. Khademhosseini, R. Langer, J. Borenstein, and J. Vacanti, *Microscale technologies for tissue engineering and biology*, *Proc Natl Acad Sci U S A* **103**, 2480 (2006).
- [4] G. Walker, H. Zeringue, and D. Beebe, *Microenvironment design considerations for cellular scale studies*, *Lab Chip* **4**, 91 (2004).
- [5] D. Breslauer, P. Lee, and L. Lee, *Microfluidics-based systems biology*, *Mol Biosyst* **2**, 97 (2006).
- [6] G. Whitesides, *The origins and the future of microfluidics*, *Nature* **442**, 368 (2006).
- [7] F. Balagaddé, L. You, C. Hansen, F. Arnold, and S. Quake, *Long- term monitoring of bacteria undergoing programmed population control in a microchemostat*, *Science* **309**, 137 (2005).
- [8] A. Groisman et al., *A microfluidic chemostat for experiments with bacterial and yeast cells.*, *Nat Methods* **2**, 685 (2005).
- [9] E. Leclerc, Y. Sakai, and T. Fujii, *Cell Culture in 3-Dimensional Microfluidic Structure of PDMS*, *Biomedical Microdevices* **5**, 109 (2003).
- [10] E. Walters, S. Clark, D. Beebe, and M. Wheeler, *Mammalian Embryo Culture in a Microfluidic Device*, in *Germ Cell Protocols*, pages 375–381, Humana Press, 2004.
- [11] A. Ben-Yakar, N. Chronis, and H. Lu, *Microfluidics for the analysis of behavior, nerve regeneration, and neural cell biology in C. elegans*, *Curr Opin Neurobiol* **19**, 561 (2009).
- [12] P. Hung, P. Lee, P. Sabounchi, R. Lin, and L. Lee, *Continuous Perfusion Microfluidic Cell Culture Array for High-Throughput Cell- Based Assays*, *Biotechnol Bioeng* **89**, 1 (2004).
- [13] M. Bennett et al., *Metabolic gene regulation in a dynamically changing environment*, *Nature* **454**, 1119 (2008).
- [14] S. Sia and G. Whitesides, *Microfluidic devices fabricated in poly(dimethylsiloxane) for biological studies*, *Electrophoresis* **24**, 3563 (2003).
- [15] J. McDonald and G. Whitesides, *Poly(dimethylsiloxane) as a material for fabricating microfluidic devices*, *Acc Chem Res* **35**, 491 (2002).
- [16] J. Lee, X. Jiang, D. Ryan, and G. Whitesides, *Compatibility of mammalian cells on surfaces of poly(dimethylsiloxane)*, *Langmuir* **20**, 11684 (2004).
- [17] T. Danino, J. Hasty, L. Tsimring, W. Mather, and O. Mondrago, *Streaming Instability in Growing Cell Populations*, *Phys Rev Lett* **104**, 208101: 1 (2010).
- [18] K. Campbell et al., *Self-Organization in High-Density Bacterial Colonies: Efficient Crowd Control*, *PLOS Biol* **5**, e302 (2007).
- [19] K. Regehr et al., *Biological implications of polydimethylsiloxane-based microfluidic cell culture*, *Lab Chip* **9**, 2132 (2009).
- [20] A. Engler, S. Sen, H. Sweeney, and D. Discher, *Matrix Elasticity Directs Stem Cell Lineage Specification*, *Cell* **126**, 677 (2006).
- [21] R. Driessen, P. Galajda, J. Keymer, and C. Dekker, *Bacterial growth and motility in sub-micron constrictions*, *Proc Natl Acad Sci U S A* **106**, 14861 (2009).
- [22] J. Drury and D. Mooney, *Hydrogels for tissue engineering : scaffold design variables*

## REFERENCES

---

- and applications*, *Biomaterials* **24**, 4337 (2003).
- [23] N. Choi et al., *Microfluidic scaffolds for tissue engineering*, *Nat Mater* **6**, 908 (2007).
- [24] M. Elowitz and S. Leibler, *A synthetic oscillatory network of transcriptional regulators*, *Nature* **403**, 335 (2000).
- [25] P. Tran, A. Paoletti, and F. Chang, *Imaging green fluorescent protein fusions in living fission yeast cells*, *Methods* **33**, 220 (2004).
- [26] J. Sulston and H. Horvitz, *Post-embryonic cell lineages of the nematode, Caenorhabditis elegans*, *Dev Biol* **56**, 110 (1977).
- [27] B. Podbilewicz and Y. Gruenbaum, *Live Imaging of Caenorhabditis elegans: Preparation of Samples*, Cold Spring Harbor Protocols, 2006.
- [28] A. Ducret et al., *A microscope automated fluidic system to study bacterial processes in real time*, *PLOS ONE* **4**, e7282 (2009).
- [29] L. Robert et al., *Predispositions and epigenetic inheritance in the Escherichia coli lactose operon bistable switch*, *Mol Syst Biol* **6**, 357 (2010).
- [30] I. Wong et al., *An agar gel membrane-PDMS hybrid microfluidic device for long term single cell dynamic study*, *Lab Chip* **10**, 2710 (2010).
- [31] S. Takeuchi, W. DiLuzio, D. Weibel, and G. Whitesides, *Controlling the shape of filamentous cells of Escherichia coli*, *Nano Lett* **5**, 1819 (2005).
- [32] J. Moffitt, B. Lee, and P. Cluzel, *The single-cell chemostat: an agarose-based, microfluidic device for high-throughput, single-cell studies of bacteria and bacterial communities*, *Lab Chip* **12**, 1487 (2012).
- [33] H. Bringmann, *Agarose hydrogel microcompartments for imaging sleep- and wake-like behavior and nervous system development in Caenorhabditis elegans larvae*, *J Neurosci Methods* **201**, 78 (2011).
- [34] T. Ahmed, T. Shimizu, and R. Stocker, *Bacterial chemotaxis in linear and nonlinear steady microfluidic gradients*, *Nano Lett* **10**, 3379 (2010).
- [35] W.-j. Chi, Y.-k. Chang, and S.-k. Hong, *Agar degradation by microorganisms and agar-degrading enzymes*, *Appl Microbiol Biotechnol* **94**, 917 (2012).
- [36] R. Pelham and Y. Wang, *Cell locomotion and focal adhesions are regulated by substrate flexibility*, *Proc Natl Acad Sci U S A* **94**, 13661 (1997).
- [37] J. Tse and A. Engler, *Preparation of hydrogel substrates with tunable mechanical properties*, in *Current protocols in cell biology*, chapter 10, John Wiley & Sons, 2010.
- [38] Y. Tanaka, K. Fukao, and Y. Miyamoto, *Fracture energy of gels*, *Eur Phys J E* **3**, 395 (2000).
- [39] D. Bonn, *Delayed Fracture of an Inhomogeneous Soft Solid*, *Science* **280**, 265 (1998).
- [40] H. Kwon, A. Rogalsky, and D.-w. Kim, *On the Measurement of Fracture Toughness of Soft Biogel*, *Polym Eng Sci* **51**, 1078 (2011).
- [41] B. Isenberg, P. Dimilla, S. Kim, and J. Wong, *Vascular smooth muscle cell durotaxis depends on substrate stiffness gradient strength*, *Biophys J* **97**, 1313 (2009).
- [42] J. Mih et al., *A Multiwell Platform for Studying Stiffness-Dependent Cell Biology*, *PLOS ONE* **6**, e19929 (2011).
- [43] J. Moorthy, R. Burgess, A. Yethiraj, and D. Beebe, *Microfluidic based platform for characterization of protein interactions in hydrogel nanoenvironments*, *Anal Chem* **79**, 5322 (2007).
- [44] S. Brahmasandra, V. Ugaz, D. Burke, C. Mastroangelo, and B. Ma, *Electrophoresis in microfabricated devices using photopolymerized polyacrylamide gels and electrode-*

- defined sample injection*, *Electrophoresis* **22**, 300 (2001).
- [45] J. Liu, S. Yang, C. Lee, and D. DeVoe, *Polyacrylamide gel plugs enabling 2-D microfluidic protein separations via isoelectric focusing and multiplexed sodium dodecyl sulfate gel electrophoresis*, *Electrophoresis* **29**, 2241 (2008).
- [46] N. Zaari, P. Rajagopalan, S. Kim, A. Engler, and J. Wong, *Photopolymerization in Microfluidic Gradient Generators: Microscale Control of Substrate Compliance to Manipulate Cell Response*, *Adv Mater* **16**, 2133 (2004).
- [47] G. Charvin, F. Cross, and E. Siggia, *A Microfluidic Device for Temporally Controlled Gene Expression and Long-Term Fluorescent Imaging in Unperturbed Dividing Yeast Cells*, *PLOS ONE* **3**, e1468 (2008).
- [48] S.-y. Cheng et al., *A hydrogel-based microfluidic device for the studies of directed cell migration*, *Lab Chip* **7**, 763 (2007).
- [49] L. Flanagan, Y.-e. Ju, B. Marg, M. Osterfield, and A. Paul, *NIH Public Access, Neuroreport* **13**, 2411 (2002).
- [50] M. Caulfield, X. Hao, G. Qiao, and D. Solomon, *Degradation on polyacrylamides Part I. Linear polyacrylamide*, *Polymer* **44**, 1331 (2003).
- [51] D. Austin et al., *Gene network shaping of inherent noise spectra*, *Nature* **439**, 608 (2006).
- [52] J. Höög et al., *Electron tomography reveals a flared morphology on growing microtubule ends*, *J Cell Sci* **124**, 693 (2011).
- [53] H. Tuson, L. Renner, and D. Weibel, *Polyacrylamide hydrogels as substrates for studying bacteria*, *Chem Commun (Camb., England)* **48**, 1595 (2012).
- [54] M. Burnham, J. Turner, D. Szarowski, and D. Martin, *Biological functionalization and surface micropatterning of polyacrylamide hydrogels*, *Biomaterials* **27**, 5883 (2006).
- [55] A. Leifer, C. Fang-yen, M. Gershow, M. Alkema, and A. Samuel, *Optogenetic manipulation of neural activity in freely moving *Caenorhabditis elegans**, *Nat Methods* **8**, 147 (2011).
- [56] K. Jensen, *The Escherichia coli K-12 "wild types" W3110 and MG1655 have an rph frameshift mutation that leads to pyrimidine starvation due to low pyrE expression levels*, *J Bacteriol* **175**, 3401 (1993).
- [57] N. Rosenfeld, J. Young, U. Alon, P. Swain, and M. Elowitz, *Gene regulation at the single-cell level*, *Science* **307**, 1962 (2005).
- [58] S. Brenner, *The Genetics of *Caenorhabditis elegans**, *Genetics* **77**, 71 (1974).
- [59] J. Crank, *The Mathematics of Diffusion*, Oxford University Press, 1956.

## REFERENCES

---

---

## Conclusion

Here, the scientific and technical implications for society of the research presented in this thesis are discussed. The two main subjects of the thesis, microbial diversity (chapters 3 and 4) and polyacrylamide devices (chapter 5) are discussed separately.

The investigation of microbial diversity and the impact of spatial structure on competitive performance within this thesis has been rather academic. It allowed to empirically validate the long standing theoretical prediction that a trade-off in growth and dispersal can promote stable coexistence of multiple species. By investigating the competition dynamics of bacterial species in porous soft agar gels, spatial confinement and segregation, reshaping selective pressures, were uncovered. Some natural habitats of bacteria, like the human gut and soil, present porous environments in which the bacteria struggle to survive. Nevertheless the competitive performance of bacteria has prior to this thesis mainly been investigated in well-stirred aquas solutions. Hence the findings presented here may be used as a starting point for future research on topics more closely impacting society. These topics include, but are not limited to, medical studies on bacterial pathogens and how they infiltrate and reside in the human gut, and agricultural studies aiming to understand the interactions between soil microbes and plants to further increase harvest yields. Fortunately, due to the fundamental nature of the research presented and the use of a simple model system, the obtained conclusions on microbial diversity hold the promise to be applicable to any biological system that grows and moves while being in a spatially structured environment.

The work on polyacrylamide devices promises to have more immediate impact on science and technology. Already now polyacrylamide devices are actively used for the study of developing nematodes. The combination of its mechanical robustness and transparency allow to follow developmental processes in single individual by time lapse microscopy. Ultimately these studies may help to understand the underlying mechanisms that make cell-fate decisions so robust even in the presence of molecular noise inherently present in many living organisms. Next to the usage of polyacrylamide devices for the study of biological systems, they may also be applied as membranes in technical solutions. Polyacrylamide membranes are permeable to small molecules, but impermeable to objects exceeding its pore size, hence it may be

## Conclusion

---

used for filtering applications, e.g. to clear water from pathogens and other unwanted components. Whether the long term stability of polyacrylamide membranes and the range of archivable pore sizes is sufficient for such applications remains to be verified.

Overall, the direct implications for society of the research presented in this thesis are rather limited. Nevertheless by exploring uncharted regions of nature future generations may benefit from these findings in ways which we cannot foresee at present.



---

## Summary

Microorganisms exhibit a fortunate combination of short life cycles and relatively simple genetic makeups while displaying a large variety of phenomena reminiscent of more complex organisms, including response to environmental factors, adaptation and even development. Nevertheless findings made with microorganisms should not be mapped one to one to higher organisms, but rather be used as a tool to uncover and probe basic principles of biology. An improved understanding of the principles of life holds the promise to unravel related but different questions in more complex life forms, including humans, in the long term.

Quantitative experiments with the ability to systematically probe the system under investigation are a key element to gain insight and understanding. In chapter 5 we presented a novel and simple technique enabling the maintenance and controlled perturbation of experimental conditions of microorganisms from bacteria to nematodes. Polyacrylamide-based devices are simple to fabricate from ingredients typically present in biolabs and are in addition biocompatible, permeable to small molecules and physically robust to even withstand adult *C. elegans* nematodes while keeping the study object within a confined region, e.g. the field of view of a microscope. Furthermore polyacrylamide gels can easily be combined with PDMS and microfluidics to continuously supply fresh nutrients and remove waste products. Beyond that we demonstrated temporal nutrient and drug shifts on bacteria and yeast. Under these conditions the dynamical response of microorganisms to well-defined environmental perturbations, e.g. change in food source, has been investigated in a setting reminiscent of the seminal work of Monod on glucose-lactose metabolism[1]. The abundance of lactose processing proteins was found to decrease after the nutrient source was shifted from lactose to glucose. While confirming previous work is an important step to validate the usefulness of a technique, opening up new routes of research is even more desirable. The use of polyacrylamide chamber to confine and study *C. elegans* nematodes makes up only a small part of chapter 5, but beyond that stimulated a variety of studies on developing nematodes ranging from embryonic development to cell lineage tracking over long time scales in single nematodes[2], most of which would not have been readily possible with previously existing techniques.

Beyond this rather technical work, we focused on questions more close to the roots of biology, i.e. what are the determining factors shaping evolution. A diverse body of recent work on simple microorganisms yielded a vast amount of insight into evolutionary dynamics (chapter 2). Ranging from detailed mapping out of evolutionary trajectories in a single gene, that demonstrated how environmental factor reshape evolutionary accessibility[3], over long term evolution studies uncovering how intermediate environments facilitate evolution[4], to the study of gene networks unveiling yet another level of interactions influencing evolution[5], evolutionary dynamics have been examined both in experiment and theory.

Realising that most of the past work had been conducted in well-stirred culture conditions[6–9] or in the absence of dispersal[10, 11], we set out to chart the influence of spatial structure and dispersal on evolutionary dynamics (chapter 3 and 4). To our surprise we found that already one of the most basic experiments imaginable, mixing two genetically identical bacterial populations labelled with distinct fluorescent markers, yielded drastically altered population dynamics in spatial habitats compared to well-mixed conditions. Motile populations in spatial habitats are found to spontaneously segregate over a broad range of initial conditions. We were able to identify dispersal rate as a key determinate of spatial confinement. Faster dispersing populations reproducibly confine slower dispersing populations and thus gain exclusive access to a subset of the nutrients enhancing their fecundity. The occurrence of spatial segregation can be rationalised by only considering nutrient consumption and the presence of a growth-dispersal trade-off. No specifically evolved direct interactions between the populations are required. The occurrence of spatial segregation is likely to be applicable to a large variety of motile species. We confirmed this generality by testing mutants of *E. coli* and *S. typhimurium*. Furthermore we were able to show in theory and experiment that these reshaped selection pressures enable stable coexistence of motile populations if the growth-dispersal trade-off is sufficiently strong. Due to its generality and simplicity we speculate that spatial segregation might have played an important role in species development in early life history. The lack of specific requirements on the environmental conditions as well as on the bacterial populations, beyond a growth-dispersal trade-off and nutrient consumption, make it accessible to very basic forms of life not able of e.g. chemical warfare.

Overall we only begin to understand the influence of dispersal and space on evolution. A next logical step to gain further insight may consist in investigating the performance of mutants arising over longer time scales and to identify whether and how long term evolutionary dynamics differ between well-stirred and spatial habitats.

---

## References

- [1] J. Monod, *Recherches sur la croissance des cultures bactériennes*, Hermann, 1942.
- [2] N. Gritti, S. Kienle, O. Filina, and J. van Zon, *Quantitative time-lapse microscopy of C. elegans development*, in preparation.
- [3] M. de Vos et al., *Environmental dependence of genetic constraint*, PLoS Genet. **9**, e1003580 (2013).
- [4] H. Lindsey et al., *Evolutionary rescue from extinction is contingent on a lower rate of environmental change*, Nature **494**, 463 (2013).
- [5] D. Segre et al., *Modular epistasis in yeast metabolism*, Nat. Genet. **37**, 77 (2005).
- [6] B. R. Levin, *Coexistence of two asexual strains on a single resource*, Science **175**, 1272 (1972).
- [7] S. Elena and R. Lenski, *Evolution experiments with microorganisms: the dynamics and genetic bases of adaptation*, Nat. Rev. Genet. **4**, 457 (2003).
- [8] J. Gore, H. Youk, and A. Van Oudenaarden, *Snowdrift game dynamics and facultative cheating in yeast*, Nature **459**, 253 (2009).
- [9] F. Poelwijk et al., *Tradeoffs and optimality in the evolution of gene regulation*, Cell **146**, 462 (2011).
- [10] B. Kerr, M. A. Riley, M. W. Feldman, and B. J. Bohannan, *Local dispersal promotes biodiversity in a real-life game of rock–paper–scissors*, Nature **418**, 171 (2002).
- [11] O. Hallatschek, P. Hersen, S. Ramanathan, and D. R. Nelson, *Genetic drift at expanding frontiers promotes gene segregation*, Proceedings of the National Academy of Sciences **104**, 19926 (2007).

## REFERENCES

---

---

## Samenvatting

Micro-organismen bezitten een gelukkige combinatie van korte levenscycli en een relatief eenvoudige genetische structuur terwijl zij een grote verscheidenheid aan verschijnselen vertonen die gelijkwaardig zijn aan meer complexe organismen. Kwantitatieve experimenten zijn een belangrijk element om inzicht en begrip te krijgen. In hoofdstuk 5 presenteerden we een techniek waarbij het onderhoud en de gecontroleerde verstoring van experimentele omstandigheden van micro-organismen van bacteriën tot nematoden mogelijk is. Bestaande uit een sandwich van glas, polyacrylamide en PDMS kan het worden vervaardigd van ingrediënten die tegenwoordig in biologische laboratoria aanwezig zijn en is het mechanisch robuust. We gebruikten het succesvol om de groeidynamiek van bacteriën, gisten en nematoden te onderzoeken onder de microscoop. Daarnaast hebben we recent werk bestudeerd over eenvoudige micro-organismen die een grote hoeveelheid inzicht opgeleverd hebben in de dynamiek van evolutionaire processen (hoofdstuk 2). Het eerdere werk is grotendeels uitgevoerd in schuddende condities. Daarom hebben we besloten om de invloed van de ruimte en dispersie op selectie te onderzoeken (hoofdstuk 3 en 4). We zagen dat selectie drastisch veranderd is in de ruimte. Ruimtelijke opsluiting en segregatie veranderen de selectiedruk. Bij een groei-dispersie tradeoff kan een stabiele coëxistentie van soorten zonder onderlinge interacties worden verkregen in ruimtelijke habitats. Deze vorm van coëxistentie vereist geen specifieke interacties en kan dus nu al toepasbaar zijn op heel primitieve levensvormen.

Kortom we beginnen pas de invloed van de dispersie en de ruimte op de evolutie te begrijpen. Veel is nog onbekend, zoals hoe langdurige evolutionaire processen worden beïnvloed door de aanwezigheid van ruimtelijke structuur.



---

## About the author

### Curriculum vitae

Sebastian Gude was born on 11.03.1985 in Kassel (Germany) and studied physics at Ludwig-Maximilians-Universität München from 2006 to 2011 graduating with a Master of Science.

### Publications

- [1] **S. Gude**, K. M. Taute, T. S. Shimizu, and S. J. Tans. Microbial diversity promoted by spontaneous spatial segregation. In preparation.
- [2] **K. M. Taute**, **S. Gude**, S. J. Tans, and T. S. Shimizu. High-throughput 3D tracking of bacteria on a standard phase contrast microscope. *Nature Communications*, 6, 2015.
- [3] **K. M. Taute**, **S. Gude**, **P. Nghe**, and S. J. Tans. Evolutionary constraints in variable environments, from proteins to networks. *Trend in Genetics*, 30:192–198, 2014.
- [4] **P. Nghe**, **S. Boulineau**, **S. Gude**, P. Recouvreur, J. S. van Zon, and S. J. Tans. Microfabricated polyacrylamide devices for the controlled culture of growing cells and developing organisms. *PLoS ONE*, 8(9):e75537, 2013.

